A Polysubstituted Ligand Framework for Color Tuning Phosphorescent Iridium(III) Complexes

Sophie A. Fitzgerald,[a] Haleema Y. Otaif,[a] Christopher E. Elgar,[a] Natalia Sawicka,[a] Peter N. Horton,[b] Simon J. Coles,[b] Joseph M. Beames,[a] and Simon J.A. Pope*[a]

[a]School of Chemistry, Main Building, Cardiff University, Cardiff CF10 3AT, Cymru/Wales, UK; [b]UK National Crystallographic Service, Chemistry, Faculty of Natural and Environmental Sciences, University of Southampton, Highfield, Southampton, SO17 1BJ, England, UK. Email: popesj@cardiff.ac.uk

Abstract

A series of ligands have been synthesized based upon a polysubstituted 2-phenylquinoxaline core structure. These ligands introduce different combinations of fluorine and methyl substituents on both the phenyl and quinoxaline constituent rings. The resultant investigation of these species as cyclometalating agents for Ir(III) gave cationic complexes of the form [Ir(C^N)$_2$(bipy)]PF$_6$ (where C^N = cyclometalating ligand; bipy = 2,2'-bipyridine). X-ray crystallographic studies were conducted on four complexes and each revealed the expected distorted octahedral geometry based upon a *cis*-C,C and *trans*-N,N ligand arrangement at Ir(III). Supporting computational studies predict that each of the complexes share the same general descriptions for the frontier orbitals. TD-DFT calculations suggest MLCT contributions to the lowest energy absorption and a likely MLCT/ILCT/LLCT nature to the emitting state. Experimentally, the complexes display tuneable luminescence across the yellow-orange-red part of the visible spectrum (λ_{em} = 579-655 nm).

Introduction

Quinoxaline compounds, which are fused nitrogen heterocyclic species, and their syntheses have been studied for many decades. This is primarily because such species have shown diverse biological activity,[1] (anti-viral, anti-bacterial and anti-inflammatory properties) and promise in treatments towards pathophysiological conditions such as epilepsy, Parkinson's and Alzheimer's.[2] Such species are not limited to biological studies: due to their highly conjugated nature, the attractive electronic properties of quinoxalines have also gathered attention in materials research as components of organic polymers for photovoltaic applications.[3]
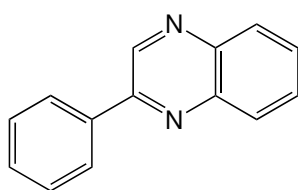
Scheme 1. The molecular structure of 2-phenylquinoxaline (2-pqx).

Functionalized quinoxalines also represent a very attractive framework for the development of ligands in coordination chemistry, including catalytic systems.[4] Their relative ease of synthesis has enabled development of a wide variety of quinoxaline-based ligands that can act as bi- or multidentate donors for different metal ions.[5] Of relevance to the current work, 2-phenylquinoxaline (2-pqx, Scheme 1) and its derivatives have been shown to be very effective cyclometalating (C^N) ligands for Ru,[6] Rh,[7] Ir [8] and Pt.[9] Of these, the studies on Ir(III) species dominate in number, many of which have been undertaken in the last few years. Typically, the resultant Ir(III) species of 2-pqx are luminescent in the red region and are thus bathochromically shifted relative to the ubiquitous $[Ir(ppy)_2(L)]^X$ (ppy = 2-phenylpyridine) analogues; the added conjugation of the 2-pqx framework can therefore modulate electronic, and redox, properties of the complexes.

General interest in cyclometalated Ir(III) species has increased significantly in the last decade.[10] It is well understood that the role of the ligands is pivotal in determining the electronic and redox properties of the resultant Ir(III) complexes and therefore the potential applications. It is interesting to note that recent work by Bernhard's group has now shown how high-throughput screening approaches can be applied to the rapid photophysical determination of a large library of heteroleptic

[Ir(C^N)$_2$(N^N)]$^+$ complexes. The study describes an accurate model for predicting emission color and suggests a framework for the rational design of complexes that could be applied to Ir(III) photocatalyst development.[11] Furthermore, our own work[12] and others,[13] have shown that machine-assisted synthesis of complexes is possible using modern laboratory technology such as flow and microwave reactors, that dramatically reduce the time taken to synthesize targets.

The growing interest and applications of Ir(III) 2-pqx complexes is attributed to the relative ease of functionality of the ligand structures and an ability to tune the electronic properties of the complexes. Many applications of Ir(III) quinoxaline complexes are now reported, including triplet sensitizers,[14] targeted photodynamic therapy reagents,[15] deep red to NIR phosphors[16] including for biological applications,[17] phosphorescent OLEDs,[18] and light emitting electrochemical cells.[19]

Our own studies have investigated Ir(III) 2-pqx species by considering different substituents on the phenyl part of the ligand.[20] Further tuning of the emission properties can be achieved through substituents on the quinoxaline ring, and led to application in triplet-triplet annihilation energy upconversion (TTA-UC),[21] wherein the Ir(III) complex acts as the photosensitizer. Targeted bioimaging studies, which make use of the low energy red emission of a peptide conjugated Ir(III) 2-pqx complex have also been successfully demonstrated.[22]

It is clear that further control over the electronic properties of Ir(III) 2-pqx complexes is advantageous for developing potential optoelectronic and photonics applications of such species. To do so requires exquisite control over the functionalization of the 2-pqx framework. Therefore, in this study, we describe a straightforward synthetic methodology for developing a hitherto unreported series of polysubstituted 2-pqx species that allow variation of substituents across both the phenyl and quinoxaline rings. This facilitates a rational approach to the modulation of Ir(III) photophysical properties using these ligands, providing significant control over the emission features of the complexes that are demonstrated to luminesce across the yellow-orange-red region of the visible spectrum.

Results and Discussion

Synthesis and characterization of polysubstituted 2-phenylquinoxalines

From a synthetic perspective, 2-pqx species can be obtained from a plethora of routes and starting materials.[23] For example, the condensation of a 2-bromoacetophenone reagent with a 1,2-phenyldiamine species is a common approach. Given that a wide range of functionalized acetophenones are commercially available, our focus was upon the use of 2-bromoacetophenone derivatives to facilitate the syntheses of 2-pqx species. To expand our ligand base, it was necessary to identify a broadly applicable brominating method for synthesizing the pre-requisite 2-bromoacetophenone species (Scheme 2). While CuBr, HBr, N-bromosuccinimide and Br$_2$ are common reagents for this purpose, they can often give mixtures of products, in particular over-brominated species, which then necessitate purification. The use of Br$_2$ often requires the co-addition of strong acids or oxidizing agents to enhance reactivity. In this study, the use of dioxane dibromide (a 1,4-dioxane compound with 1:1 bromine) as a solid form brominating reagent which can be easily handled and avoids the use of co-reagents to the reaction was investigated.[24]

Thus, portion-wise addition of dioxane dibromide over 10 minutes at room temperature to a stirring solution of the chosen acetophenone in dioxane gave mono-bromination of the acetyl group in moderate-to-excellent yields. ^{1}H NMR spectra of the reaction products showed loss of the original methyl signal, and the appearance of a new aliphatic singlet resonance at 4.35-4.85 ppm consistent with the formation of the bromo-acetyl functional group. There was no evidence of dibrominated side products.
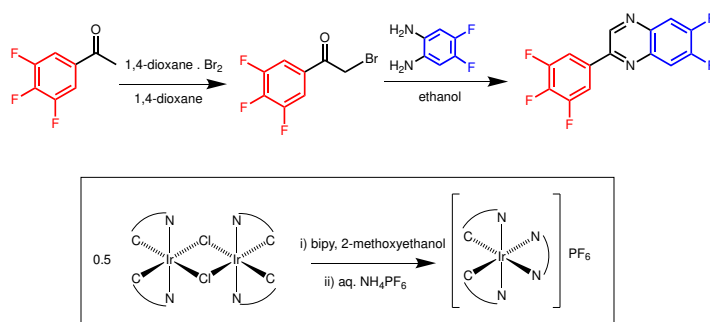
Scheme 2. Synthetic route to the polysubstituted quinoxaline ligands using **LH^{10}** as the example. Inset: general route to the Ir(III) complexes.
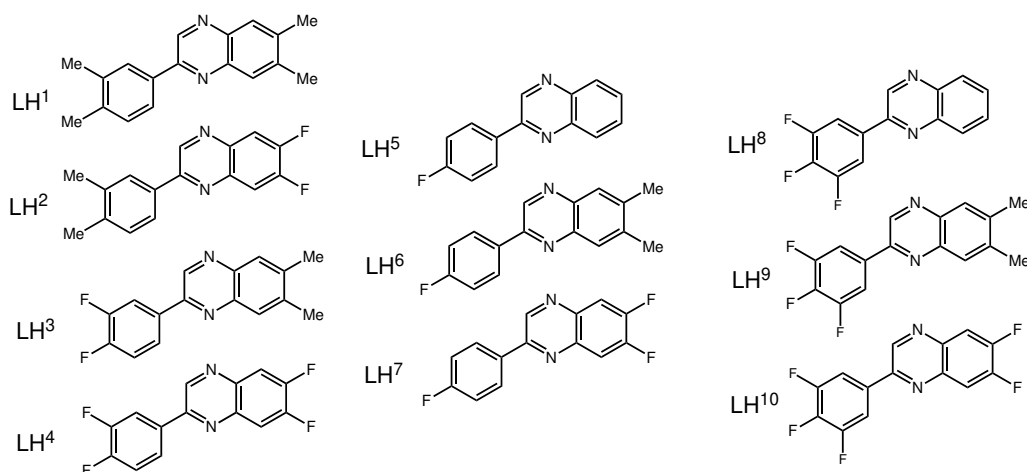
**Scheme 3**. Structures of the ten 2-pqx species synthesized in this study.

The 2-bromoacetophenone variants were then heated to reflux in ethanol with either 1,2-phenylenediamine, 4,5-difluoro-1,2-phenylenediamine or 4,5-dimethyl-1,2-phenylenediamine to form the corresponding 2-pqx ligands (**LH[1-10]**) in good yields (Scheme 3). The majority of these quinoxalines are novel apart from **LH[5]** and **LH[6]**, which have been reported previously. [25,26] Thus, ten ligands with variable electronic character within both the phenyl and quinoxaline constituents were produced. It should be noted that the trifluorophenyl moiety is a relatively uncommon donor unit for Ir(III), but has been incorporated into 2-phenylpyridine type ligands.[27]

The new ligands were characterized using a range of spectroscopic and analytical techniques. [1]H, ^{13}C, and where appropriate, ^{19}F NMR spectroscopies were particularly helpful. In all cases, the quinoxaline heterocycle was identified in ^{1}H NMR spectra via a new singlet around 9.20 ppm assigned to the proton at the C3 position of the quinoxaline ring. For **LH[1]**, **LH[2]**, **LH[6]** and **LH[9]**, characteristic methyl resonances were also observed in the aliphatic region at 2.3-2.6 ppm (Table 1). ^{19}F{^{1}H} NMR spectroscopy provided helpful information on the fluorine environment(s) within **LH[2-10]** (Table 2). The data shows that the fluorine substituents attached to the quinoxaline ring tend to be more deshielded than those on the phenyl ring. In most cases the unsymmetrical nature of the ligands leads to coupling between adjacent fluorines with typical $^3J_{FF}$ values around 19-22 Hz. A comparison of the ^{19}F resonances for **LH[3]** and **LH[6]** clearly demonstrates the influence of adding an adjacent fluorine substituent to the phenyl ring, with ca. 25 ppm upfield shift induced by the second fluorine; this is further exemplified by the trifluorophenyl derivatives (**LH[8-10]**). ^{13}C{^{1}H} NMR spectra of the trifluoro derivatives, **LH[8-10]**, each gave a signature doublet of triplets ($^1J_{CF} \sim 250$

Hz, $^2J_{CF} \sim 10$ Hz) pattern for the fluorine substituted carbon at the 4-position of the phenyl ring. Satisfactory high resolution mass spectrometry (HRMS) data were obtained for each new 2-pqx ligand.

Synthesis and characterization of the Ir(III) complexes

All ligands, **LH$^{1-10}$**, were investigated as potential cyclometalating agents with Ir(III). The synthetic methodology was based upon previous reports.[28] Firstly, reaction with hydrated IrCl$_3$ gave the dimeric species, [{Ir(**L^n**)$_2$(μ-Cl)}$_2$], as a series of colored solids. These dimeric species were subsequently used in a further reaction step with 2 eq. 2,2'-bipyridine (bipy), splitting the dimer and forming the target monometallic complexes, [Ir(**L^n**)$_2$(bipy)]PF$_6$ (Scheme 2). Further purification was required using column chromatography (silica gel) and products were isolated as beige or red colored solids.
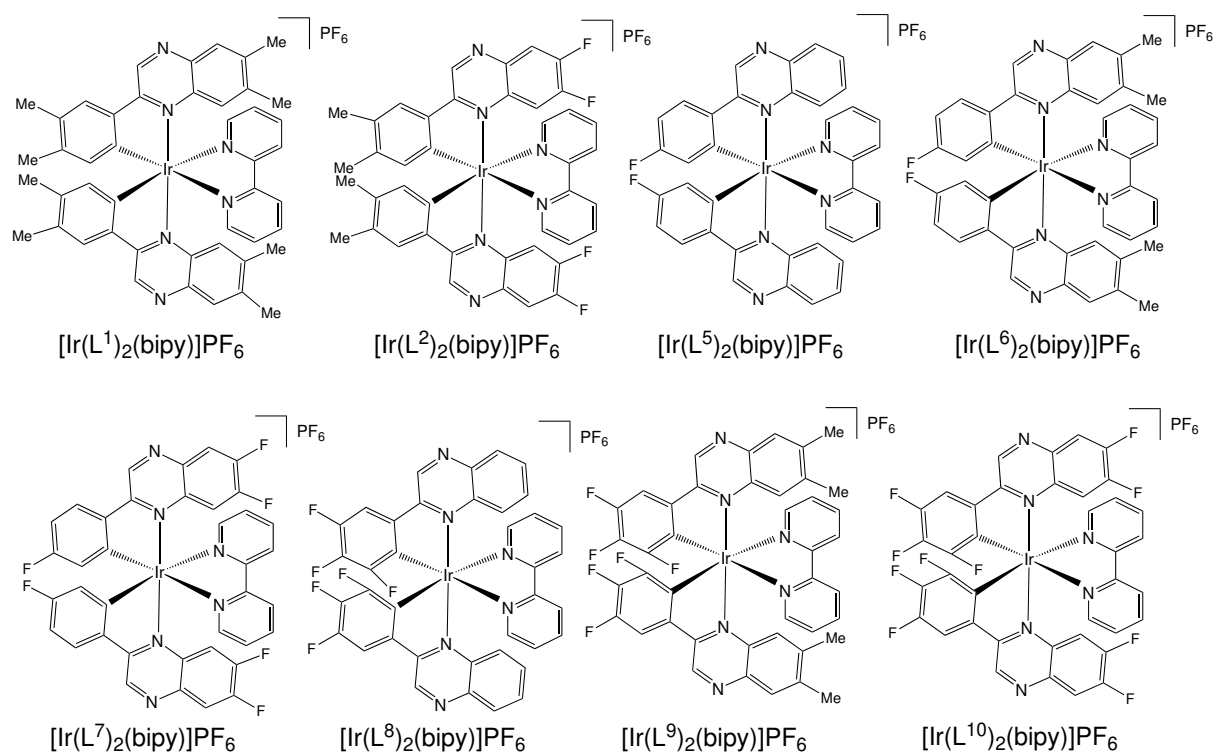
Scheme 4. The structures of the iridium(III) complexes successfully isolated during the study.

The majority of the complexes (Scheme 4) were successfully isolated using this methodology. However, in our hands, despite repeated chromatographic purification steps, it was not possible to obtain spectroscopically pure samples of $[Ir(L^3)_2(bipy)]PF_6$ or $[Ir(L^4)_2(bipy)]PF_6$; both complexes are based upon the difluorophenyl-derived ligands and are discussed later.

Table 1. A comparison of the methyl group ^1H NMR resonances for the methylated ligands and complexes.

	$CH_3\ \delta_H$ / ppm[a] (ligand)	$CH_3\ \delta_H$ / ppm[a] (complex)
LH^1	2.36, 2.40, 2.52 (overlapping 6H)	1.75, 1.95, 2.27, 2.33
LH^2	2.37, 2.40	1.99, 2.29
LH^6	2.52, 2.53 [b]	1.76, 2.31 [c]
LH^9	2.52 (overlapping 6H)	1.67, 2.17

[a] All spectra obtained in $CDCl_3$ unless otherwise indicated; [b] spectra obtained in $(CD_3)_2CO$; [c] spectra obtained in CD_3CN.

Firstly, discussion will focus on the characterization of the successfully isolated complexes. For example, formation of $[Ir(L^1)_2(bipy)]PF_6$ was fully supported by ^1H NMR spectroscopy. The symmetry of the complex renders both cyclometalating ligands as equivalent and therefore four unique methyl resonances were resolved in the aliphatic region between 1.75 – 2.23 ppm (Table 1). The effect of coordination to Ir(III) induces a small, but general upfield shift and a greater inequivalence among the methyl groups. In the aromatic region the effect of cyclometalation results in five singlet resonances associated with L^1. The most upfield aromatic resonance was ca. 6.2 ppm and is indicative of the proton environment adjacent to the metalated carbon of the ligand (Scheme 4 and Figure S1, SI). This was observed for all complexes other than $[Ir(L^{8-10})_2(bipy)]PF_6$ where the ligand is fluorinated at the carbon adjacent to the coordinated carbon. In all cases, the most downfield quinoxaline ring singlet shifted to around 9.8 ppm, again indicative of coordination.

For $[Ir(L^6)_2(bipy)]PF_6$ the inequivalence of the two methyl environments was clearly indicated by ^1H NMR spectroscopy, with two distinct singlets at 1.76 and 2.31 ppm. This again suggests that upon coordination to the Ir(III) center, one of the quinoxaline methyl groups becomes more shielded compared to the free ligand. Subsequent elucidation of the solid-state structures (see later) suggests that this

shielding may be due to the orientation of one of the methyl groups with respect to the bipy ligand.
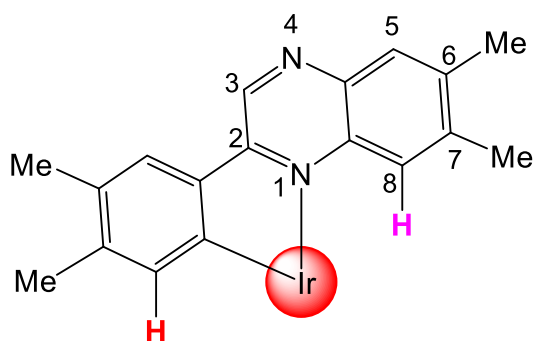
Scheme 5. A representation of the coordination of **L¹** with Ir(III) identifying the four unique methyl environments, the relatively shielded proton environments (in red and pink), and the numbering convention for the quinoxaline moiety.

In all relevant cases, $^{19}F\{^1H\}$ NMR spectral data were obtained and indicated a general downfield shift (Table 2) *versus* the free ligands, consistent with a withdrawal of electron density from the ligand upon coordination. In [Ir(**L**$^{8\text{-}10}$)$_2$(bipy)]PF$_6$, upon coordination the three fluorine substituents on the phenyl ring become inequivalent. Supporting HRMS data was obtained for all complexes (*e.g.* Figure S2, SI) revealing the parent cation in each case with an appropriate isotopic distribution for iridium.

Table 2. A comparison of the $^{19}F\{^1H\}$ NMR data for the successfully isolated fluorinated Ir(III) complexes *versus* the corresponding free ligands. Data for hexafluorophosphate anions is omitted.

	Free ligand δ_F ($^3J_{FF}$) / ppm	*Complex δ_F ($^3J_{FF}$) / ppm*
LH²	-129.8 (d, 20 Hz), -131.0 (d, 20 Hz)	-123.8 (d, 22 Hz), -128.6 (d, 22 Hz)
LH³	-135.8 (d, 21 Hz), -136.4 (d, 21 Hz)	Not isolated
LH⁴	-128.63 (d, 21 Hz), -129.32 (d, 21 Hz),	Not isolated
	-134.28 (d, 21 Hz), -135.77 (d, 21 Hz)	
LH⁵	-109.9 (s)	-103.6 (s)
LH⁶	-111.2 (s)	-103.9 (s)
LH⁷	-109.9 (s),	-106.5 (s),
	-129.2 (d, 21 Hz), -130.1 (d, 21 Hz)	-128.6 (d, 22 Hz), -133.1 (d, 22 Hz)
LH⁸	-132.6 (d, 20 Hz),-157.5 (t, 20 Hz)	-127.1 (dd, 22, 6 Hz),

LH⁹	-132.9 (d, 21 Hz), -158.2 (t, 21 Hz)	-142.2 (dd, 22, 6 Hz), -156.0 – -156.2 (m) -127.3 (dd, 22, 6 Hz), -142.7 (dd, 22, 6 Hz), -157.0 (dd, 22, 6 Hz)
LH¹⁰	-128.1 (d, 21 Hz), -128.5 (d, 21 Hz), -132.3 (d, 20 Hz), -156.7 (t, 21 Hz)	-126.9 (dd, 22, 6 Hz), -127.9 (d, 22 Hz), -131.4 (d, 22 Hz), -141.7 (dd, 19, 6 Hz), -154.9 – -155.0 (m)

As noted earlier, the reactions of **LH³** and **LH⁴** yielded impure complexes. Firstly, numerous attempts to purify putative [Ir(**L³**)₂(bipy)]PF₆ using recrystallisation approaches and column chromatographic techniques failed. Informatively, the ¹H NMR spectrum of the crude sample of [Ir(**L³**)₂(bipy)]PF₆ showed four methyl resonances, none of which were consistent with the presence of free ligand, and a complicated aromatic region: the anticipated C_2 symmetry of the complex should produce two methyl environments. Similarly, the ¹⁹F{¹H} NMR spectrum also showed more resonances than expected, but again all shifts were different to the free ligand. HRMS data on crude [Ir(**L³**)₂(bipy)]PF₆ showed a single cluster of peaks at *m/z* 887.2097, which was consistent with the expected formulation of [Ir(**L³**)₂(bipy)]PF₆. Taken together it seems feasible that the desired complex has formed in the proposed stoichiometry, but that a mixture of isomers was present in the sample.
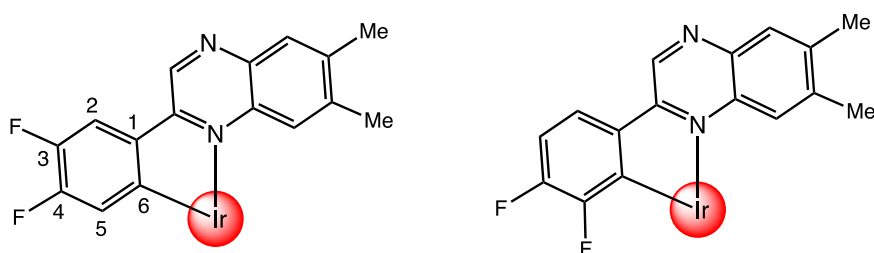
Scheme 6. The different C^N cyclometalation modes available to **L³**.

Since there are two potential sites of *ortho*-metalation, at either the 2- or 6-position of the phenyl ring (Scheme 6), it appears that both are accessible using the adopted reaction conditions for the precursor dimer. Very similar observations were noted in our attempts to isolate [Ir(**L⁴**)₂(bipy)]PF₆: the presence of numerous resonances in the ¹⁹F{¹H} NMR spectrum again suggestive of a mixture of isomers in the sample. Since the corresponding complexes of **LH¹** and **LH²** gave single isomer products it is likely

that the differences in steric demand of Me versus F induce these contrasting outcomes.

The X-ray crystal structures of [Ir(L^1)$_2$(bipy)]PF$_6$, [Ir(L^2)$_2$(bipy)]PF$_6$, [Ir(L^5)$_2$(bipy)]PF$_6$ and [Ir(L^6)$_2$(bipy)]PF$_6$

Single crystals were obtained for [Ir(L^1)$_2$(bipy)]PF$_6$ (dark red, shard-shaped), [Ir(L^2)$_2$(bipy)]PF$_6$ (dark red, rod-shaped), [Ir(L^6)$_2$(bipy)]PF$_6$ (orange, block-shaped) and [Ir(L^5)$_2$(bipy)]PF$_6$ (red, plate-shaped) following either vapor diffusion of diethyl ether in to a dichloromethane or chloroform solution of the complex, or slow evaporation from a MeCN solution ([Ir(L^6)$_2$(bipy)]PF$_6$). Data collection parameters are presented in Table S1, SI.

In each case the obtained structures (Figures 1 and 2) confirmed the expected coordination sphere at iridium, with the quinoxaline derived ligands coordinating in a cyclometalating mode, resulting in a *cis*-C,C and *trans*-N,N coordination arrangement at Ir(III).[29] The monocationic complex unit is charge balanced by the presence of one hexafluorophosphate counter ion. In each case there were solvents of crystallisation; for [Ir(L^5)$_2$(bipy)]PF$_6$ there was a partial amount of disordered water present for which solvent masking was employed. For [Ir(L^1)$_2$(bipy)]PF$_6$ and [Ir(L^2)$_2$(bipy)]PF$_6$ the dimethyl-substituted phenyl ring is coordinated to Ir(III) via the 6-position, in a manner that minimizes unfavorable steric clashes. For [Ir(L^1)$_2$(bipy)]PF$_6$ the structure also reveals that on each quinoxaline ring a methyl substituent lies directly above the plane of the aromatic bipy ligand: the distance of C35 to the plane of the (C29-C34) ring is 3.565(14) Å, with distance to ring centroid of 3.605(14) Å. The proximity of this arrangement may explain the observations from the ^{1}H NMR data wherein one of the methyl environments is relatively shielded. Selected bond lengths and bond angles for all the structures are shown in Table S2, SI and all Ir-C and Ir-N distances fall in the typical range of complexes of this type.[20]
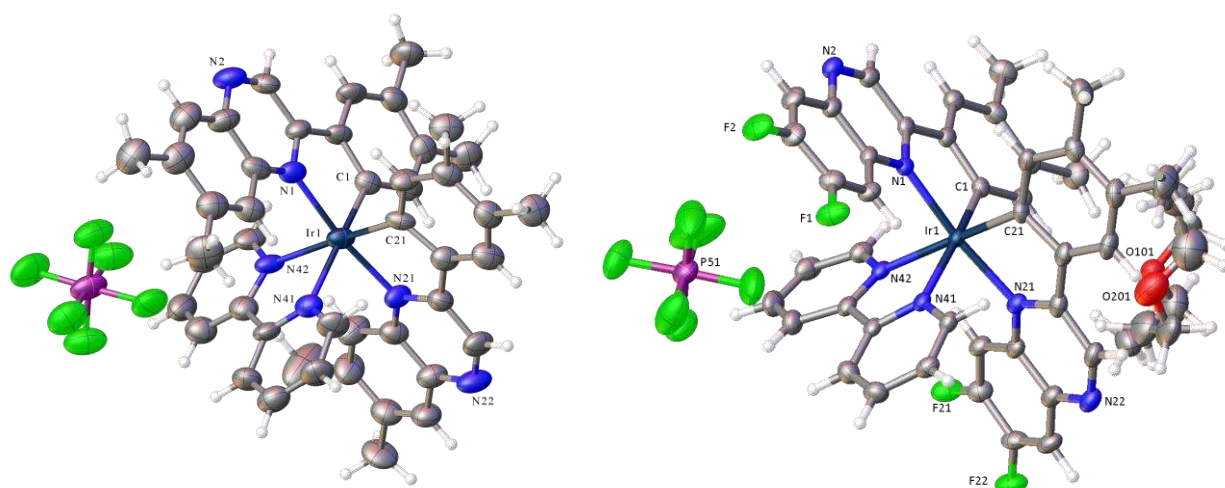
Figure 1. X-ray structures of [Ir(**L¹**)₂(bipy)]PF₆ (left) and [Ir(**L²**)₂(bipy)]PF₆ (right).
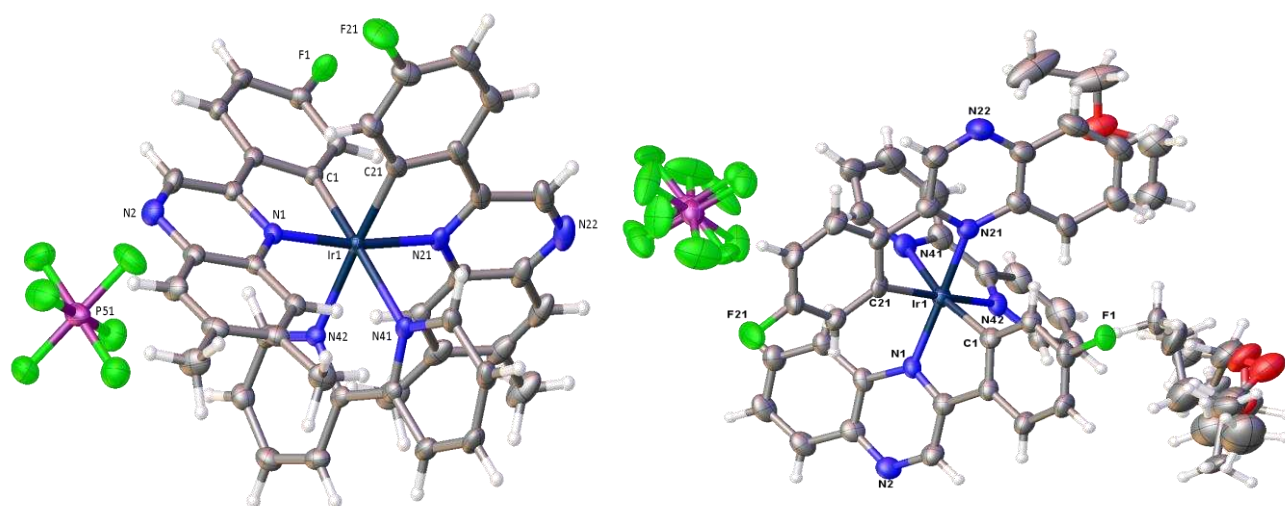
Figure 2. X-ray structures of [Ir(**L⁵**)₂(bipy)]PF₆ (left) and [Ir(**L⁶**)₂(bipy)]PF₆.

Computational studies: Density Functional Theory

To probe the effect of the ligand substituents on the electronic structure and the optical properties of [Ir(**Lⁿ**)₂(bipy)]⁺, density functional theory (DFT) calculations were performed on each of complexes. All calculations were undertaken using the B3LYP functional with a 6-31G* basis set, and an SDD ECP for the central iridium atom. Calculations were performed within an implicit acetonitrile solvent, consistent with the spectroscopic measurements. Geometries of the complexes were optimized using the prior method, and the resulting minimum energy structures compared against X-ray

crystallographic data where available to demonstrate the suitability of the method. The geometrical structures of iridium(III) complexes obtained from the DFT optimizations for [Ir(**L^1**)$_2$(bipy)]PF$_6$ and [Ir(**L^2**)$_2$(bipy)]PF$_6$ are in superb agreement with crystallographic data (Figure 3).
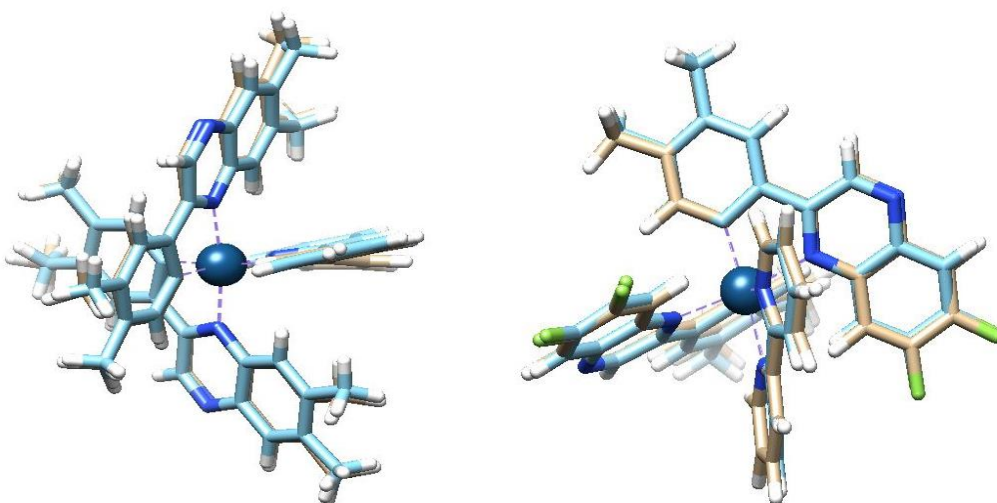
Figure 3. Overlay of the crystal structures (blue) and DFT//B3LYP/6-31G*(SDD) optimized structures (brown) for [Ir(**L^1**)$_2$(bipy)]$^+$ (left) and [Ir(**L^2**)$_2$(bipy)]$^+$ (right).

Molecular orbital decomposition was performed on each of the experimentally isolated versions of complex, using a basis of each individual ligand, as well as the central iridium atom. This analysis (Table 3) predicts that the occupied molecular orbitals in these Ir complexes have a significant metallic *d*-orbital character whilst the unoccupied molecular orbitals are predominantly ligand-centered. In all cases, the HOMO is composed of almost equal contributions from the metal center (32-35%) and from each quinoxaline ligand (Q1/Q2), and negligible contribution from bipy (2%). For the LUMOs, the two quinoxalines form pairs of pseudo-degenerate orbitals with alternating contributions from each of the of the quinoxalines: *e.g.* the [Ir(**L^1**)$_2$(bipy)]$^+$ LUMO is comprised of contributions of 50% and 44% from the quinoxalines, Q1 and Q2 respectively, whilst the LUMO+1 shows the reverse (Q1 = 44%; Q2 = 50%). The metal contribution to the unoccupied orbitals is negligible. The bipy ligand is also predicted to contribute little to the LUMO or LUMO+1, to which we attribute the majority of the longer wavelength photoexcitation bands, although it is the dominant contributor to the LUMO+2 orbital (96%). The significant change in iridium *d*-orbital contribution

12

to the electronic character of the HOMO compared to the LUMO/LUMO+1 (and indeed even to higher lying unoccupied orbitals) suggests that the singlet excited states have a significant degree of metal-to-ligand charge transfer (MLCT) character.

Table 3. A summary of the major calculated contributions to each MO from each part of the complex. Q1 and Q2 are the quinoxaline ligands.

Complex	Ir 5d		Q1		Q2		bipy
	HOMO-1	HOMO	LUMO	LUMO+1	LUMO	LUMO+1	LUMO+2
$[Ir(L^1)_2(bipy)]^+$	4	32	50	44	44	50	95
$[Ir(L^2)_2(bipy)]^+$	4	32	63	31	31	64	96
$[Ir(L^5)_2(bipy)]^+$	8	35	48	48	47	48	96
$[Ir(L^6)_2(bipy)]^+$	5	32	50	45	45	50	96
$[Ir(L^7)_2(bipy)]^+$	6	33	41	54	54	41	96
$[Ir(L^8)_2(bipy)]^+$	4	34	48	47	47	48	97
$[Ir(L^9)_2(bipy)]^+$	2	32	48	47	46	47	97
$[Ir(L^{10})_2(bipy)]^+$	2	33	47	48	48	48	96
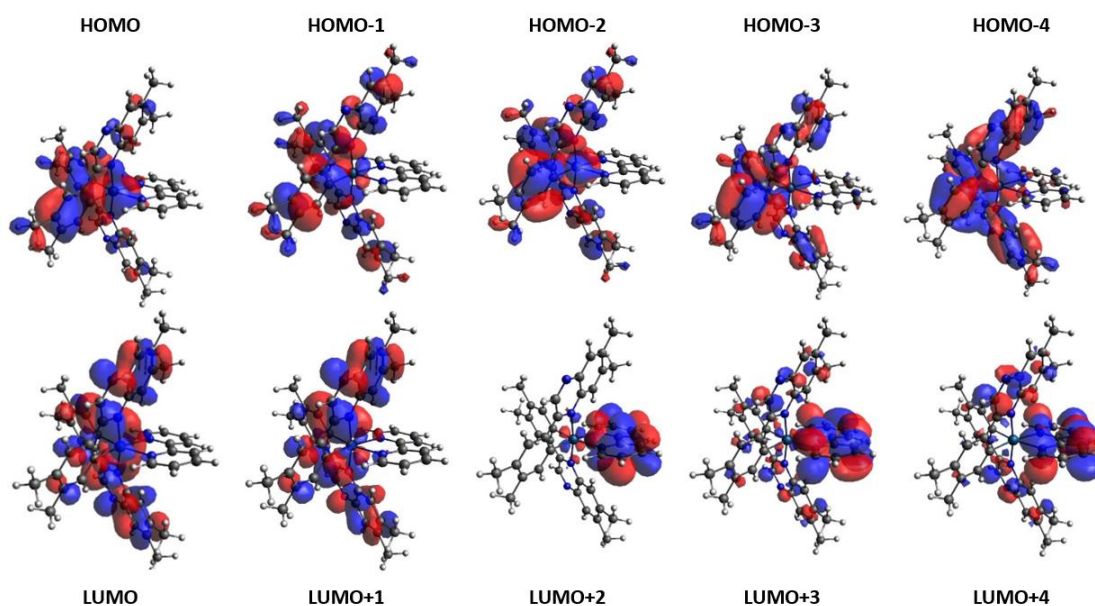
Figure 4. Calculated Kohn-Sham frontier molecular orbitals for $[Ir(L^1)_2(bipy)]^+$. Frontier orbitals for $[Ir(L^{2-10})_2(bipy)]^+$ can be found in Figures S3-S9, SI.

To estimate the vertical excitation energies of the low-lying singlet and triplet excited states of the complexes, TD-DFT calculations using the CAM-B3LYP functional were carried out from the optimized ground-state geometries. In each case, the lowest 30 singlet-to-singlet spin-allowed and thirty singlet-to-triplet spin-forbidden transitions

were calculated and compared with the absorption spectra. The non-relativistic nature of the calculations means that we predominantly examine the spin-allowed transitions, but can use the spin-forbidden excitation energies to suggest absorption band character. In all cases the calculated transitions were in reasonable agreement with experimental absorption spectra discussed later (Table 4 and Figure 4). In the case of [Ir(**L^1**)$_2$(bipy)]$^+$, the lowest spin-forbidden $S_o \rightarrow T_1$ transition was predicted to occur at 544 nm, attributed to a ^{3}MLCT transition which may become weakly allowed due to spin–orbit coupling effects. These transitions correlate well with the broad, structureless and somewhat weak feature observed in the experimental absorption spectrum at 550 nm, discussed later.

The most important singlet transitions of [Ir(**L^1**)$_2$(bipy)]$^+$ and their associated oscillator strengths and configurations are summarized in Table 4, with analogous data for [Ir(**L$^{2-10}$**)$_2$(bipy)]$^+$ shown in Tables S3-S9, SI. The longest wavelength singlet excitation is expected to be intense HOMO to LUMO+1 transition at 409 nm (f=0.2089), followed at higher energy by an intense HOMO to LUMO transition at 403 nm, suggesting ^{1}MLCT charge transfer in these shorter wavelength transitions. Again, this is in good agreement with the structured absorption features between 350 nm $< \lambda$ < 400 nm in the experimental spectrum. TD-DFT also predicts intense transitions between 350 nm $< \lambda < 300$ nm, including transitions with complex and mixed ^{1}ILCT/ ^{1}LLCT/ ^{1}MLCT characters. In the high-energy region ($\lambda < 300$ nm), the calculations indicate that in addition to ligand centered ^{1}(π-π*) transition, ^{1}ILCT/ ^{1}LLCT/ ^{1}MLCT have some contributions.

Table 4. A description of the calculated MO contributions, excited state descriptions and their associated transitions for [Ir(L^1)$_2$(bipy)]$^+$ complex (Q1 and Q2 are the different 2-pqx ligands; bipy = bipyridine).

Orbital	Moiety Contribution to Orbital (%)				Orbital Contribution to Excited State	
	Ir (5d)	bipy	Q1	Q2	Excited State	Contributing Transitions (> 10 %)
LUMO +4	1	76	12	11	1 (409 nm f=0.2089)	HOMO-1 → LUMO (10%)
LUMO +3	2	80	9	9		HOMO → LUMO+1 (83%)
LUMO +2	2	96	1	1	2 (403 nm f=0.0588)	HOMO-1 → LUMO+1 (11%)
LUMO +1	4	2	44	50		HOMO → LUMO (83%)
LUMO	4	2	50	44		
HOMO	32	2	33	33	3 (348 nm f=0.183)	HOMO → LUMO+2 (88%)
HOMO -1	4	1	47	47		
HOMO -2	10	1	45	45	4 (331 nm f=0.1855)	HOMO -2 → LUMO (26%)
HOMO -3	20	3	39	39		HOMO -1 → LUMO +1 (55%)
					5 (330 nm f=0.2751)	HOMO-2 → LUMO+1 (25%)
HOMO -4	22	4	39	35		HOMO -1 → LUMO (53%)

Table 5. Computed values for the absorption and emission maxima of the experimentally isolated Ir(III) complexes. Experimentally determined emission wavelength maxima shown in parentheses.

Complex	$S_o \rightarrow S_1$ Abs. / nm	$S_o \rightarrow T_n$ Abs. / nm	$T_1 \rightarrow S_o$ Em. / nm
[Ir(L^1)$_2$(bipy)]$^+$	409	544	694 (628)
[Ir(L^2)$_2$(bipy)]$^+$	419	563	712 (655)
[Ir(L^5)$_2$(bipy)]$^+$	385	502	664 (590)
[Ir(L^6)$_2$(bipy)]$^+$	383	496	662 (585)
[Ir(L^7)$_2$(bipy)]$^+$	390	510	670 (594)
[Ir(L^8)$_2$(bipy)]$^+$	377	493	582 (579)
[Ir(L^9)$_2$(bipy)]$^+$	375	486	583 (584)
[Ir(L^{10})$_2$(bipy)]$^+$	381	501	585 (583)

Comparison of DFT optimized singlet and triplet excited-state geometries afford the computation of the lowest energy spin-forbidden band positions without requiring the use of TD-DFT. This method was used to compute the vertical spin-forbidden emission band of all complexes, and the results are shown in Table 5. This method affords a good qualitative insight into the effect of ligand structure on the spectral properties of the complexes. In particular, the predicted $T_1 \rightarrow S_0$ wavelengths exhibit the correct trend throughout the series. Although this approach tends to systematically

underestimate the spin-forbidden transition energies, the values calculated for [Ir($\mathbf{L^{8-10}}$)$_2$(bipy)]$^+$ are remarkably well matched to experimental data.

Table 6. Calculated energies of the frontier orbitals of the iridium(III) complexes and their differences.

Complex	HOMO energy (eV)	LUMO energy (eV)	ΔE
[Ir($\mathbf{L^1}$)$_2$(bipy)]$^+$	-5.62	-2.54	3.08
[Ir($\mathbf{L^2}$)$_2$(bipy)]$^+$	-5.76	-2.77	2.99
[Ir($\mathbf{L^5}$)$_2$(bipy)]$^+$	-6.03	-2.74	3.29
[Ir($\mathbf{L^6}$)$_2$(bipy)]$^+$	-5.95	-2.64	3.31
[Ir($\mathbf{L^7}$)$_2$(bipy)]$^+$	-6.1	-2.86	3.24
[Ir($\mathbf{L^8}$)$_2$(bipy)]$^+$	-6.15	-2.88	3.27
[Ir($\mathbf{L^9}$)$_2$(bipy)]$^+$	-6.08	-2.77	3.31
[Ir($\mathbf{L^{10}}$)$_2$(bipy)]$^+$	-6.22	-3.00	3.22

TD-DFT calculations were used to investigate the effects of quinoxaline ligand substitution pattern on electronic properties. As presented in Table 6, the calculations predict that substitution of either phenyl or quinoxaline constituents can affect both HOMO and LUMO energy levels (there is an interplay between the units), but that the phenyl moiety is predicted to have a greater impact on HOMO and LUMO energy levels and thus optical properties. For example, destabilization of the HOMO (achieved by methylating the phenyl donor) and stabilization of the LUMO (achieved by fluorinating the quinoxaline) are represented by [Ir($\mathbf{L^2}$)$_2$(bipy)]$^+$ which is predicted to possess the smallest band gap. As discussed later, this is reflected in the largest bathochromic shift in the emission wavelength and the shortest lifetime (*cf.* Energy Gap rule). Conversely, sequential fluorination of the phenyl donor is predicted to result in a progressive stabilization of the HOMO level and thus a blue shift in the emission wavelengths. Trifluorination of the phenyl donor combined with a methylated quinoxaline unit is thus predicted to give the largest band gap.

UV-visible absorption and fluorescence properties of the ligands

The electronic properties of the free ligands (**LH$^{1-10}$**) were obtained in aerated acetonitrile solution at room temperature. The UV-vis. absorption spectra (for example, Figure 5) showed a range of π-π* transitions < 375 nm which are associated with different aromatic entities. Increasing the degree of methylation on the phenyl

ring resulted in a bathochromic shift in the absorption features. Fluorination of the quinoxaline had a smaller effect on the absorption spectra.
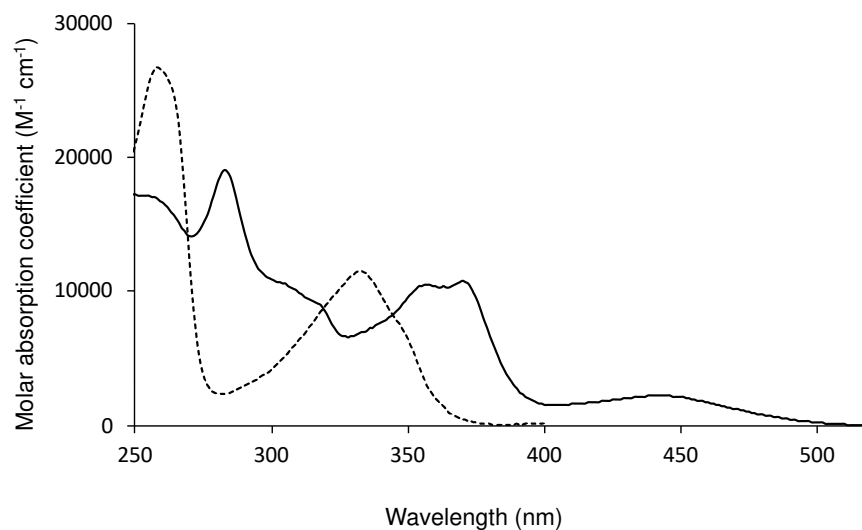

Figure 5. Example UV-vis. absorption spectra (MeCN) comparing **LH[8]** (dashed line) and [Ir(**L[8]**)$_2$(bipy)]PF$_6$ (solid line).

UV-vis. absorption and emission properties of the complexes

The data associated with UV-vis. absorption wavelengths is shown in Table 7 and Figure 5. There are three general regions of absorption: firstly, higher energy features at 230-320 nm with a high molar absorption coefficient, secondly a moderately intense feature at 320-400 nm, and finally a weaker broad feature > 400 nm. A comparison with the free ligand data implies that the bands observed 230-400 nm are associated with ligand centered transitions $\pi \rightarrow \pi^*$, which are bathochromically shifted upon coordination to Ir(III). Across the series of complexes, it is the position of the longest wavelength band that varies appears most sensitive to the variation in ligand structure. Prior studies on related Ir(III) complexes have attributed these features to MLCT features; typically, the broadness of these features can be attributed to both spin allowed and spin forbidden contributions, the latter facilitated by the heavy Ir atom (iridium possesses the largest spin-orbit coupling constant [30] of any metal in the *d* block). In general, the presence of fluorine substituents on the phenyl ring results in a significant blue shift of the MLCT features relative to the methylated variants. This is in agreement with the TD-DFT calculations discussed earlier and can be related to the contribution of the phenyl orbitals to the HOMO. A comparison of [Ir(**L[1]**)$_2$(bipy)]PF$_6$ and [Ir(**L[2]**)$_2$(bipy)]PF$_6$ also demonstrates that addition of fluorine substituents to the quinoxaline ring red shifts the absorption band, consistent with previous reports on 2-

pqx complexes of Ir(III).[31] As discussed earlier, the supporting DFT calculations suggest that the compositions of the important HOMO and LUMOs do not vary greatly with the ligand structure, but rather the relative energies of the frontier orbitals are modulated by the ligand substituents. These predictions and the relative trends are supported by the experimental UV-vis. absorption data. Thus, as predicted by DFT, the most red-shifted absorption is represented by [Ir($\mathbf{L^2}$)$_2$(bipy)]PF$_6$, which combines the dimethylated phenyl donor (raising the HOMO) and the difluorinated quinoxaline (lowering the LUMO). Conversely, this analysis implies that a (poly)fluorinated phenyl donor combined with a dimethylated quinoxaline fragment should provide a blue-shifted absorption. Again, the spectroscopic data shows that trifluorination of the phenyl donor ([Ir($\mathbf{L^{8-10}}$)$_2$(bipy)]PF$_6$) gave the most blue-shifted MLCT features in the visible region.

Table 7. Absorbance and luminescence data for the isolated Ir(III) complexes.[a]

Complex	λ_{abs} ($\varepsilon \times 10^4$ M^{-1} cm^{-1}) / nm[b]	λ_{em} / nm[c]	Aerated τ / ns[d]	Degassed τ / ns[d]	Φ [e]
[Ir($\mathbf{L^1}$)$_2$(bipy)]PF$_6$	485 sh (0.4), 378 (1.7), 293 (3.1), 267 (3.5)	628	253	1886	0.03
[Ir($\mathbf{L^2}$)$_2$(bipy)]PF$_6$	518 sh (0.4), 373 (2.1), 292 (3.1), 266 (3.6)	655	215	659	0.01
[Ir($\mathbf{L^5}$)$_2$(bipy)]PF$_6$	460 sh (0.2), 359 (0.7), 288 (2.4), 249 (2.7)	590	430	3416	0.04
[Ir($\mathbf{L^6}$)$_2$(bipy)]PF$_6$	450 sh (0.7), 372 (2.4), 286 (4.9)	585	446	4872	0.08
[Ir($\mathbf{L^7}$)$_2$(bipy)]PF$_6$	449 sh (0.4), 362 (1.6), 284 (2.5), 259 (2.9)	594	571	1387	0.09
[Ir($\mathbf{L^8}$)$_2$(bipy)]PF$_6$	442 sh (0.2), 370 (1.8), 357 (1.1), 283 (1.9), 241 (1.8)	579	747	5322	0.08
[Ir($\mathbf{L^9}$)$_2$(bipy)]PF$_6$	439 (0.7), 379 (2.9), 363 (2.2), 284 (4.6), 239 (4.3)	584	612	6518	0.10
[Ir($\mathbf{L^{10}}$)$_2$(bipy)]PF$_6$	440 sh (0.2), 372 (1.0), 360 (1.0), 280 (1.6), 239 (1.8)	583	535	1446	0.11

[a] All measurements obtained at room temperature in aerated MeCN; [b] 1×10^{-5} M; [c] λ_{ex} = 450 nm; [d] observed lifetime, λ_{ex} = 295 or 355 nm; [e] quantum yield, versus standard [Ru(bipy)$_3$](PF$_6$)$_2$ in MeCN standard (Φ = 0.016), λ_{ex} = 450 nm.

Emission spectra of each of the complexes (Figure 6) were obtained in aerated acetonitrile at ambient temperature with λ_{ex} = 355 nm. The complexes all exhibit a broad emission profile comparable to those of the previously reported complexes bearing 2-phenylquinoxaline ligands. The bands are typically featureless and broad, with only the hypsochromically shifted variants displaying subtle vibronic features.

As expected, the onset and emission peak maxima are dependent on the nature and the position of substituents located on the cyclometalated ligands, with peak tuning demonstrated between 579 nm < λ < 655 nm. The trends observed in the UV-vis. absorption data are mirrored here: complexes that are fluorinated on the phenyl moiety, $[Ir(L^{5-10})_2(bipy)]PF_6$, show a relative hypsochromic shift compared to their methyl-substituted analogues, $[Ir(L^1)_2(bipy)]PF_6$ and $[Ir(L^2)_2(bipy)]PF_6$. These experimental observations were nicely predicted by the DFT calculations (Table 5) describing the trends in $T_1 \rightarrow S_0$ transition energies. It is noteworthy that the substitution on the phenyl ring in cyclometalated ligand leads to a more profound shift in the emission bands while the substitution on the quinoxaline moiety provides a much finer tuning parameter. Thus, when utilized in tandem there is significant tunability of the photophysics afforded by this polysubstituted ligand framework.

The observed lifetimes are typical of phosphorescent complexes in aerated solution with values of 215-747 ns, wherein the peak emission energy seems to strongly correlate with lifetime; the longest wavelength emitters, $[Ir(L^1)_2(bipy)]PF_6$ and $[Ir(L^2)_2(bipy)]^+$, exhibit the shortest phosphorescence lifetimes, which accords with the Energy Gap Law. The supporting quantum yields are up to ca. 11 % in aerated solution, which indicates potential utility in applications, such as bioimaging, where good emissive properties are advantageous in oxygenated media.[32] As shown in Table 7, the fluorinated-phenyl complexes in aerated solutions show a significant increase in the lifetimes and quantum yields comparing with their methylated counterparts. Under deoxygenated conditions the complexes all showed elongated lifetimes (Figure S10, SI), which in some cases were significantly increased (Table 7) to several microseconds. The magnitudes of these lifetimes are consistent with the reduction in $^3O_2$ quenching, affording the definitive assignment that the emissive state is triplet in character. Low temperature (77K) data were also obtained for the complexes (MeCN glass) and showed emission spectra that were closely reminiscent of the room temperature profiles as well as replicating the trends within the series (Figure S11, SI).

The photophysical data for the Ir(III) complexes support the assignment of a phosphorescent state that is dominated by charge transfer character. In line with other well-known d-block lumophores, ^{3}MLCT character contributes to the emission, and our supporting DFT studies also predict that ILCT/LLCT (localized on the 2-pqx ligands) make important contributions in these complexes. Thus the functionalization at both the phenyl and quinoxaline moieties of the 2-pqx ligand yields excellent tuning of the emission colors of the complexes.

Comparison of these characteristics with the benchmark complex [Ir(ppy)(bipy)]$^+$ reveal some similarities and clear differences. In aerated MeCN, the [Ir(ppy)(bipy)]$^+$ emission properties[10i] (λ_{em} 602 nm, ϕ_{em} 9.3%, τ_{obs} 275 ns), attributed to a mixed ^{3}MLCT/^{3}LLCT transition, are broadly comparable with some of the complexes described here. For [Ir(ppy)$_2$(bipy)]$^+$ the HOMO has been described as comprising both Ir and phenyl character and is thus directly comparable to the 2-pqx Ir(III) complexes under discussion. However, in contrast, the LUMO of [Ir(ppy)$_2$(bipy)]$^+$ is predicted to be exclusively localised on the bipy ligand.[33] These differences emphasize the design principles of the 2-pqx based complexes described herein.
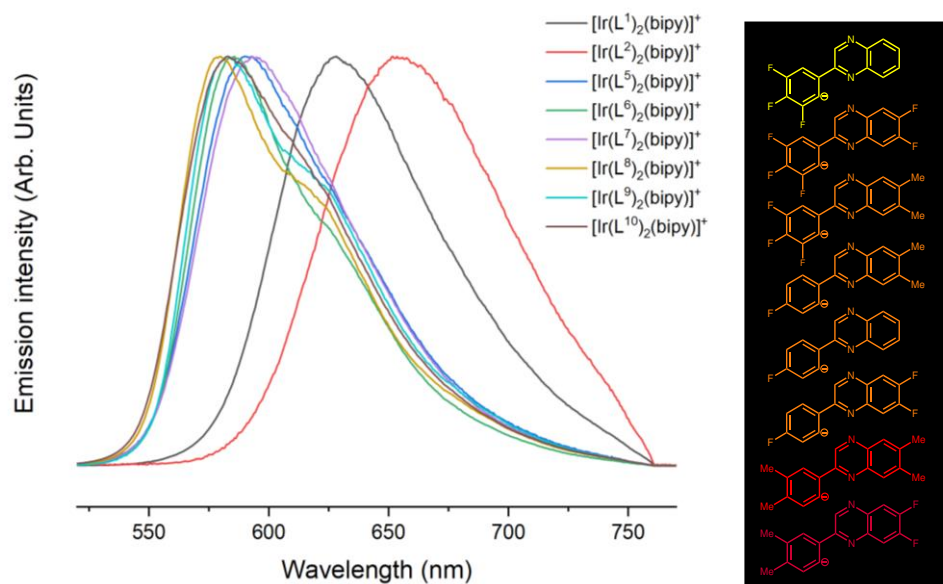

Figure 6. Normalized emission spectra recorded for all isolated Ir(III) complexes (293 K, MeCN, 10^{-5} M).

Transient Absorption Spectroscopy and Kinetics

Nanosecond transient absorption (TA) of all Ir(III) complexes were again recorded in aerated acetonitrile using a pump wavelength of 355 nm and are shown in Figure 7. The general spectral appearance of all eight complexes are nearly identical and are very similar to the related Ir(III) complexes previously reported.[32] The complexes all feature a ground state bleach in the shorter wavelength spectral region (350 nm $< \lambda <$ 400 nm), ascribed to the pump-driven depletion of the ground state ^{1}MLCT absorption band. This ground-state bleaching splits into a doublet in the fluorinated-phenyl complexes, but does not form this doublet structure in their methylated counterparts. The spectra also exhibit strong increases in optical density in the regions 410 nm $< \lambda <$ 435 nm and 550 nm $< \lambda <$ 670 nm, assigned to triplet – triplet absorption bands ($T_1 \rightarrow T_n$ transitions), with the longer wavelength triplet absorption feature becoming significantly more intense and better resolved in the fluorinated-phenyl complexes.
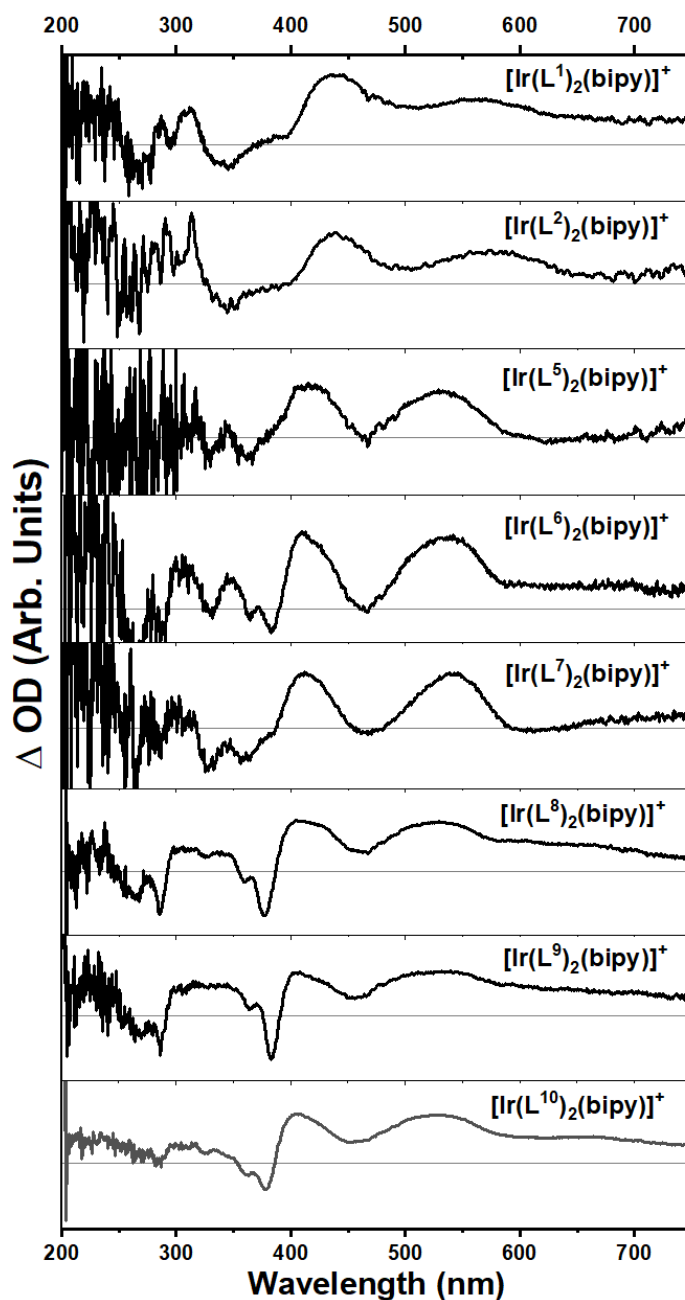
Figure 7. Background subtracted transient absorption spectra of all complexes in acetonitrile, λ_{exc} = 355 nm. The grey line represents $\Delta OD = 0$ in all cases.

As observed in Figure 7, each complex exhibits analogous TA features that shift depending on the substituted cyclometalated ligand used. The spectral features in the transient absorption spectra also follow the same ordering as the emission spectra with respect to their band positions, with [Ir(L^2)$_2$(bipy)]PF$_6$ displaying features at longer

wavelengths *versus* [Ir($\mathbf{L^{5-10}}$)$_2$(bipy)]PF$_6$ at shorter wavelengths. In all cases we assign the transient absorption spectra to a linear combination of ground state bleaching and T$_1$ – T$_n$ excited state absorption bands. To further confirm this assignment, the transient absorption spectrum of [Ir(L^8)$_2$(bipy)]$^+$ was simulated through combination of a linear combination of a bleach taken from the inverse of the absorption spectrum shown in figure 5 and the computed T$_1$ – T$_n$ excited state absorption bands. The excited state absorption bands were generated from a TD-DFT calculation using the optimized [Ir($\mathbf{L^8}$)$_2$(bipy)]$^+$ T$_1$ geometry as the reference state. Thirty excited states were included in the calculation, and the relative band intensities were taken directly and are not altered in the simulation. A 50 nm convolution of the line spectrum was applied to mimic the breadth of the bands. Using this approach there was excellent agreement between the simulated (Figure S12, SI) and experimental transient spectra with just a slight shift in the position of the TD-DFT computed transitions.

The transient kinetics of all major TA features of the [Ir($\mathbf{L^1}$)$_2$(bipy)]PF$_6$ and [Ir($\mathbf{L^6}$)$_2$(bipy)]PF$_6$ complexes are shown in Figure 8 (and Figures S13-S15, SI); all observable transitions decay monoexponentially. Within each of the datasets for complex [Ir($\mathbf{L^1}$)$_2$(bipy)]PF$_6$ and [Ir($\mathbf{L^6}$)$_2$(bipy)]PF$_6$, the kinetic data suggest that all the features exhibit similar decay lifetimes, suggesting that they all originate from the same excitation and intersystem crossing processes that produce an emissive ^{3}MLCT state. There is no evidence of fluorescence within these spectra.
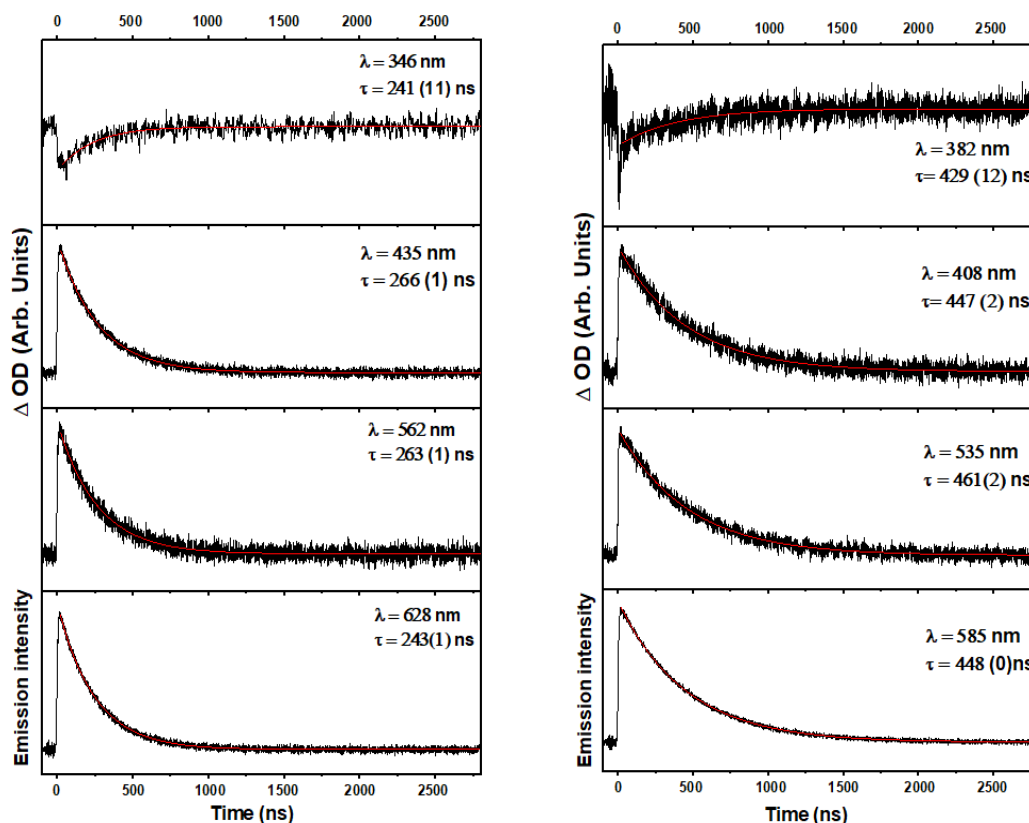
Figure 8. Kinetic traces of the major features of the transient spectra of [Ir(**L**^{1})$_2$(bipy)]PF$_6$ (left) and [Ir(**L**^{6})$_2$(bipy)]PF$_6$ (right) complexes in acetonitrile at room temperature, aerated. Wavelengths and lifetimes of each trace are inset.

Conclusions

Dioxane dibromide is an excellent brominating reagent applicable to a range of substituted acetophenones allowing a series of polysubstituted 2-phenylquinoxaline species to be synthesized. This synthetic approach now allows control over the electronic character of both the phenyl and quinoxaline donor consistuents of the 2-pqx ligands. The different substitution patterns of the ligands thus facilitate excellent tuning of the phosphorescent emission wavelengths of the Ir(III) complexes ranging from yellow to deep red wavelengths. Through a combination of spectroscopic and computational analyses, these complexes are shown to demonstrate a significant MLCT/LLCT/ILCT character to their emission properties. This is achieved by modulation of both HOMO (Ir and phenyl donor) and LUMO (quinoxaline) energies via ligand substitution. Previous studies have shown that additional tuning of emissive bis-cyclometalated Ir(III) complexes can be achieved using the ancillary ligand, which can

often directly contribute to the LUMO level. However, our studies on 2-pqx complexes of Ir(III) has shown that ancillary ligands, such as 2,2'-bipyridine, picolinate or pyrazinoate, primarily influence the HOMO energy level; they do not provide important contributions to the LUMO.[32] Therefore it is reasonable to assume that a similar effect could be employed for the complexes described herein providing further subtle tuning of spectral properties.

The ability to easily tune emission characteristics of such Ir(III) species is key to diverse, and ever-expanding optoelectronic and photoredox applications. For example, the development of deep red emitters is a highly active area of research within the study of organometallic phosphors for materials and biological applications.[34] Traditionally many Ir(III) complexes that are successfully utilized in OLED devices[35] tend to be neutral species, such as [Ir(C^N)$_3$] or [(Ir(C^N)$_2$(L^X)], and further studies could consider the investigation of related homoleptic [Ir(2-pqx)$_3$] species based upon the types of ligands described herein. However, it is noteworthy that significant recent progress has also been achieved with sublimable cationic Ir(III) species[36] including the use of bulky counter anions,[37] suggesting that the Ir(III) species described herein could have promise in such applications.

Experimental Section

General Experiments. All commercially available reagents were used as received. Caution is advised when handling dioxane dibromide [38] (CAS 15481-39-7; not to be confused with 1,4-dioxane dibromide, CAS 21992-70-1) as it is a flammable solid and should be treated accordingly. ^{1}H, ^{19}F{^{1}H} and ^{13}C{^{1}H} NMR spectra were recorded on an NMR-FT Bruker 500 and 400 MHz spectrometer and recorded in CDCl$_3$, acetone-d_6, acetonitrile-d_3 and DMSO-d_6. ^{1}H and ^{13}C{^{1}H} NMR chemical shifts (δ) were determined relative to residual solvent peaks with digital locking and are given in ppm. Coupling constants are quoted in Hz. Low-resolution mass spectra were obtained by the staff at Cardiff University. High-resolution mass spectra were carried out at the EPSRC National Mass Spectrometry Facility at Swansea University. UV-Vis studies were performed on a Shimadzu UV-1800 spectrophotometer as MeCN solutions (1 × 10^{-5} M). Photophysical data were obtained on a JobinYvon–Horiba Fluorolog spectrometer fitted with a JY TBX picosecond photodetection module as MeCN

solutions. Emission spectra were uncorrected and excitation spectra were instrument corrected. The pulsed source was a Nano-LED configured for 295 or 459 nm output operating at 1 MHz. Luminescence lifetime profiles were obtained using the JobinYvon–Horiba FluoroHub single photon counting module and the data fits yielded the lifetime values using the provided DAS6 deconvolution software. Quantum yield measurements were obtained on aerated MeCN solutions of the complexes using [Ru(bipy)$_3$](PF$_6$)$_2$ in aerated MeCN as a standard (Φ = 0.016).[39] Spectra and lifetime measurements made at 77 K were performed using an Oxford Instruments Optistat DN2 variable temperature liquid nitrogen cryostat.

Transient absorption measurements

Transient absorption measurements were performed using an Edinburgh Instruments LP920 spectrometer. Spectra were collected using a pump wavelength of 355 nm (third harmonic of a Continuum Surelite II Nd:YAG laser system). The probe for these measurements was a Xenon lamp, with spectra available between 300 < λ < 800 nm. Wavelength dependent spectra were recorded with a 2.05 nm spectral resolution, from an Andor ICCD camera, integrated over the first 500 ns after the pump laser pulse. Spectra are shown as $\Delta OD_{Xe\ lamp}$, referred simply as ΔOD. Lifetime data was generated using a photomultiplier to collect time resolved signals, with the bandwidth of these data being identical to the camera resolution (2.05 nm). Lifetime data is fit using the Origin 2020 software package, and each data set is fit using a monoexponential function, with no evidence of multiexponential components. Lifetime uncertainties are obtained from a standard Least-Squares fitting algorithm.

Computational methods

Electronic structure calculations were performed using density fitted-density functional theory within the Gaussian 09 computational chemistry suite,[40] using the Stuttgart-Dresden (SDD) effective core potential and basis set in the treatment of the iridium,[41] with a 6-31G* basis set for all lighter atoms.[42] Cationic complex geometry optimizations were performed using the self-consistent reaction field model (SCRF), treating the solvent implicitly as a dielectric continuum. As described earlier, the solvent chosen was acetonitrile. Acetonitrile is characterized by an electrical permittivity (ε) of 35.688 within the calculations. This models the solvent as

surrounding a cavity in which the solute resides, with the cavity characterized by an integral equation formalism for the polarizable continuum model (IEFPCM).

Geometry optimizations were performed using an ultrafine grid and very tight convergence criteria, with minima by the calculation of harmonic vibrational frequencies, in all cases demonstrating no imaginary frequencies. These stationary points were used in single point TD-DFT calculations to compute vertical excitation energies. All TD-DFT calculations were undertaken using a linear response approach. All TD-DFT calculations were also performed with a long range corrected hybrid functional (CAM-B3LYP).

Phosphorescence and spin-forbidden absorption bands were investigated using unrestricted density functional theory to compute parameters associated with the first triplet state (T_1). Decomposition of the molecular orbital character was performed using the GaussSum software package.[43] Crystal structure overlays with optimised computational structures has been performed using the Chimera software package, which has also been used to calculate root mean squared deviation (RMSD) values for these comparative structures.[44]

X-ray crystallography

Data collection and processing

Suitable crystals of $[Ir(L^1)_2(bipy)]PF_6$, $[Ir(L^2)_2(bipy)]PF_6$, $[Ir(L^5)_2(bipy)]PF_6$ and $[Ir(L^6)_2(bipy)]PF_6$ were selected and data collected following a standard method.[45] In each case, a crystal was selected and mounted on a MITIGEN holder in perfluoroether oil on either a Rigaku 007HF diffractometer equipped with Varimax confocal mirrors and an AFC11 goniometer and HyPix 6000 detector (for $[Ir(L^1)_2(bipy)]PF_6$), or a Rigaku FRE+ diffractometer equipped with VHF Varimax confocal mirrors and an AFC12 goniometer and HyPix 6000 detector (for $[Ir(L^2)_2(bipy)]PF_6$, $[Ir(L^5)_2(bipy)]PF_6$ and $[Ir(L^6)_2(bipy)]PF_6$). The crystals were kept at a steady T = 100(2) K during data collection using an Oxford Cryosystems low-temperature device. The structures were solved with the ShelXT[46] structure solution program using the Intrinsic Phasing solution method and by using Olex2[47] as the graphical interface. The models were refined with version 2018/3 of ShelXL[48] using Least Squares minimisation.

CCDC2090298-2090301 contains supplementary X-ray crystallographic data for [Ir(L^1)$_2$(bipy)]PF$_6$, [Ir(L^2)$_2$(bipy)]PF$_6$, [Ir(L^5)$_2$(bipy)]PF$_6$ and [Ir(L^6)$_2$(bipy)]PF$_6$ respectively. This data can be obtained free of charge via http://www.ccdc.cam.ac.uk/conts/retrieving.html, or from the Cambridge Crystallographic Data Centre, Union Road, Cambridge, CB2 1EZ; fax(+44) 1223-336-033 or email: deposit@ccdc.cam.ac.uk.

Synthesis of the ligand precursors

Preparation of 2-bromo-(3,4-dimethylphenyl)ethan-1-one [49]
Slow addition of dioxane dibromide (1.840 g, 1.1 eq, 7.425 mmol) in a solution of 1,4-dioxane (20 mL) and diethyl ether (20 mL) to 3,4-dimethylacetophenone (1.000 g, 0.998 mL, 6.747 mmol) in the same solvent mixture, took place at room temperature with stirring for 2 h. The pale yellow solution was added to water and extracted with diethyl ether. The combined ether layers were dried over MgSO$_4$. The solvent was reduced *in vacuo*, a minimum amount of hexane was added, and the resultant suspension was filtered under suction to give the product as an off-white solid. Yield = 1.364 g, 89 %.

Preparation of 2-bromo-(3,4-difluorophenyl)ethan-1-one [50]
As above, but using 3,4-difluoroacetophenone (1.00 g, 0.803 mL, 6.405 mmol) and dioxane dibromide (1.747 g, 1.1 eq, 7.046 mmol). Yield = 0.311 g, 21 %.

Preparation of 2-bromo-(4-fluorophenyl)ethan-1-one [51]
As above, but using 4'-fluoroacetophenone (3.00 g, 2.63 mL, 21.7 mmol) and dioxane dibromide (5.92 g, 1.10 eq, 24.0 mmol) to give the brominated product as white crystals. Yield = 2.51 g, 53 %.

Preparation of 2-bromo-(3,4,5-trifluorophenyl)ethan-1-one [52]
As above, but using 3,4,5-trifluoroacetophenone (1.00 g, 0.751 mL, 5.743 mmol) and dioxane dibromide (1.566 g, 1.10 eq, 6.317 mmol) to give the brominated product as a yellow oil. Yield = 1.45 g, 99 %.

Synthesis of the 2-phenylquinoxaline ligands

Preparation of 2-(3,4-dimethylphenyl)-6,7-dimethylquinoxaline (LH^1)

2-bromo-3,4-dimethylacetophenone (0.799 g, 3.520 mmol) and 4,5-dimethyl-1,2-phenylenediamine (0.528 g, 3.870 mmol) were heated to reflux in ethanol (10 mL) for 24 h in an inert nitrogen atmosphere. The mixture was then filtered under reduced pressure and washed with a small amount of ethanol and hexane. Yield = 0.374 g, 41 %. ^{1}H NMR (400 MHz, CDCl$_3$) δ_H = 9.20 (s, 1H), 7.97 (d, $^4J_{HH}$ = 0.9 Hz, 1H), 7.90 (s, 1H), 7.88 (dd, $^3J_{HH}$ = 7.8, $^4J_{HH}$ 1.7 Hz, 1H), 7.84 (s, 1H), 7.31 (d, $^3J_{HH}$ = 7.8 Hz, 1H), 2.51 (overlapping, 6H), 2.40 (s, 3H), 2.36 (s, 3H) ppm. ^{13}C{^{1}H} NMR (101 MHz, CDCl$_3$) δ_C = 142.7, 140.8, 139.0, 137.7, 134.9, 130.5, 128.8, 128.7, 128.3, 125.0, 20.6, 20.5, 20.2, 19.9 ppm. FTIR (solid, cm^{-1}) (ATR) ν_{max}: 2972, 2945, 2907, 1628, 1605, 1570, 1528, 1483, 1447, 1362, 1317, 1283, 1234, 1209, 1121, 1053, 1022, 1003, 991, 964, 943, 885, 862, 837, 794, 737, 716, 637, 623, 546, 488, 442, 428. UV-vis (MeCN): λ_{max} ($\epsilon \times 10^4$ /L mol^{-1} cm^{-1}) 214 (4.5), 265 (3.3), 348 (1.8) nm. HR MS (EI+): *m/z* calc'd 262.1470 for C$_{18}$H$_{18}$N$_2$; found 262.1465 [M+H]$^+$.

Synthesis of 2-(3,4-dimethylphenyl)-6,7-difluoroquinoxaline (LH^2)

As with **LH^1**, but using 2-bromo-3,4-dimethylacetophenone (0.998 g, 4.395 mmol) and 4,5-difluoro-1,2-phenylenediamine (760 mg, 1.2 eq, 5.274 mmol) to give the product as an off-white solid. Yield = 0.593 g, 50 %. ^{1}H NMR (400 MHz, CDCl$_3$) δ_H = 9.27 (s, 1H), 7.96 (d, $^4J_{HH}$ = 0.6 Hz, 1H), 7.88 (dd, $^3J_{HF}$ = 7.9, $^4J_{HF}$ = 5.5 Hz, 2H), 7.86 – 7.81 (m, 1H), 7.32 (d, $^3J_{HH}$ = 7.9 Hz, 1H), 2.40 (s, 3H), 2.37 (s, 3H) ppm. ^{13}C{^{1}H} NMR (101 MHz, CDCl$_3$) δ_C = 152.4 (d, $^2J_{CF}$ = 3.1 Hz), 145.7 (d, $^2J_{CF}$ = 3.2 Hz), 139.9, 137.9, 133.9, 130.7, 128.7, 125.1, 115.2 (dd, $^2J_{CF}$ = 17.2 Hz, $^3J_{CF}$ = 1.6 Hz), 115.0 (dd, $^2J_{CF}$ = 17.2 Hz, $^3J_{CF}$ = 1.6 Hz), 20.2, 20.0 ppm. ^{19}F{^{1}H} NMR (376 MHz, CDCl$_3$) δ_F = -129.8 (d, $^3J_{FF}$ = 20 Hz), -131.0 (d, $^3J_{FF}$ = 20 Hz) ppm. FTIR (solid, cm^{-1}) (ATR) ν_{max} : 3067, 2978, 2922, 1636, 1609, 1545, 1493, 1449, 1433, 1385, 1350, 1315, 1283, 1225, 1167, 1165, 1128, 1051, 1016, 988, 968, 926, 880, 862, 835, 752, 731, 710, 650, 613, 602, 546, 492, 463, 440. UV-vis (MeCN): λ_{max} ($\epsilon \times 10^4$ /L mol^{-1} cm^{-1}) 213 (5.5), 256 (2.9), 343 (1.9) nm. HR MS (EI+): *m/z* calc'd 270.0969 for C$_{16}$H$_{12}$F$_2$N$_2$; found 270.0970 [M+H]$^+$.

Synthesis of 2-(3,4-difluorophenyl)-6,7-dimethylquinoxaline (LH^3)

As with **LH¹**, but using 2-bromo-3,4-difluoroacetophenone (0.311 g, 1.320 mmol) and 4,5-dimethyl-1,2-phenylenediamine (0.216 g, 1.2 eq, 1.586 mmol) to give the product as a pale yellow solid. Yield = 0.209 g, 58 %. ^{1}H NMR (400 MHz, CDCl$_3$) δ_H = 9.17 (s, 1H), 8.07 (ddd, $^3J_{HH}$ = 11.4, $^4J_{HF}$ = 7.7, $^4J_{HH}$ = 2.2 Hz, 1H), 7.93 – 7.89 (m, 1H), 7.89 (s, 1H), 7.86 (s, 1H), 7.37 – 7.30 (m, 1H), 2.52 (overlapping, 6H) ppm. ^{13}C{^{1}H} NMR (101 MHz, CDCl$_3$) δ_C = 141.8, 141.5, 141.3, 140.9, 128.8, 128. 4, 124.0 – 123.3 (m), 117.7 (dd, $^1J_{CF}$ = 151.8 Hz, $^2J_{CF}$ = 17.0 Hz), 117.4 (dd, $^1J_{CF}$ = 139.6, $^2J_{CF}$ = 17.7 Hz) 20.5, 20.4 ppm. ^{19}F{^{1}H} NMR (376 MHz, CDCl$_3$) δ_F = -135.8 (d, $^3J_{FF}$ = 21 Hz), -136.4 (d, $^3J_{FF}$ = 21 Hz) ppm. FTIR (solid, cm^{-1}) (ATR) v$_{max}$: 3040, 2978, 2355, 1616, 1604, 1520, 1518, 1487, 1472, 1442, 1369, 1364, 1323, 1290, 1273, 1254, 1213, 1188, 1165, 1113, 1049, 1007, 1003, 976, 939, 897, 876, 829, 773, 710, 638, 583, 492, 457, 434. UV-vis (MeCN): λ_{max} ($\varepsilon \times 10^4$ /L mol^{-1} cm^{-1}) 203 (3.1), 262 (3.6), 340 (1.4) nm. HR MS (EI+): *m/z* calc'd 270.0969 for C$_{16}$H$_{12}$F$_2$N$_2$; found 270.0969 [M+H]$^+$.

*Synthesis of 2-(3,4-difluorophenyl)-6,7-difluoroquinoxaline (**LH⁴**)*

As with **LH¹**, but using 2-bromo-3,4-difluoroacetophenone (1.505g, 6.404 mmol) and 4,5-difluoro-1,2-phenylenediamine (0.923 g, 1.0 eq, 6.404 mmol) to give the product as an off-white solid. Yield = 0.450 g, 25 %. ^{1}H NMR (400 MHz, CDCl$_3$) δ_H = 9.25 (s, 1H), 8.08 (ddd, $^3J_{HF}$ = 11.2, $^3J_{HH}$ 7.6 Hz, $^4J_{HF}$ 2.2 Hz, 1H), 7.95 – 7.90 (m, 1H), 7.87 (ddd, $^3J_{HF}$ = 10.2, $^4J_{HF}$ = 8.1 Hz, $^5J_{HH}$ = 2.0 Hz, 1H), 7.40 – 7.32 (m, 2H) ppm. ^{13}C{^{1}H} NMR (101 MHz, CDCl$_3$) δ_C = 154.6 – 153.4 (m), 153.0 – 150.7 (m), 150.0 – 149.8 (m), 142.8 (d, $^3J_{CF}$ = 3.3 Hz), 140.0 – 138.6 (m), 133.4 (dd, $^3J_{CF}$ = 5.8, $^4J_{CF}$ = 3.9 Hz), 123.8 (dd, $^3J_{CF}$ = 6.7, $^4J_{CF}$ = 3.6 Hz), 117.6 (dd, $^1J_{CF}$ = 145.8 Hz, $^2J_{CF}$ = 18.3 Hz), 115.3 (dd, $^2J_{CF}$ = 17.3 Hz, $^3J_{CF}$ = 1.8 Hz), 115.1 (dd, $^2J_{CF}$ = 17.3 Hz, $^3J_{CF}$ = 1.9 Hz) ppm. ^{19}F{^{1}H} NMR (376 MHz, CDCl$_3$) δ_F = -128.6 (d, $^3J_{FF}$ = 21 Hz), -129.3 (d, $^3J_{FF}$ = 21 Hz), -134.3 (d, $^3J_{FF}$ = 21 Hz), -135.8 (d, $^3J_{FF}$ = 21 Hz) ppm. FTIR (solid, cm^{-1}) (ATR) v$_{max}$: 3042, 1636, 1609, 1508, 1476, 1445, 1410, 1350,1300, 1281, 1273, 1233, 1223, 1188, 1124, 968, 901, 889, 818, 779, 731, 706, 660, 611, 581, 494, 492, 451, 399. UV-vis (MeCN): λ_{max} ($\varepsilon \times 10^4$ /L mol^{-1} cm^{-1}) 207 (3.6), 253 (2.5), 334 (1.4) nm. HR MS (EI+): *m/z* calc'd 278.0467 for C$_{14}$H$_6$F$_4$N$_2$; found 278.0470 [M+H]$^+$.

*Synthesis of 2-(4-fluorophenyl)-6,7-dimethylquinoxaline (**LH⁶**)*

As with **LH¹**, but using 2-bromo-4-fluoroacetophenone (1.00 g, 4.61 mmol) and 4,5-dimethyl-1,2-phenylenediamine (753 mg, 1.2 eq, 5.53 mmol) to give the product as a yellow solid. Yield = 0.58 g, 50 %. ^{1}H NMR (400 MHz, d$_6$-acetone) δ_H = 9.38 (s, 1H), 8.42 – 8.36 (m, 2H), 7.87 (s, 1H), 7.85 (s, 1H), 7.39 – 7.33 (m, 2H), 2.53 (s, 3H), 2.52 (s, 3H) ppm. ^{13}C{^{1}H} NMR (101 MHz, CDCl$_3$) δ_C = 164.2 (d, $^1J_{CF}$ = 250.2 Hz), 150.2, 142.2, 141.3, 141.2, 140.6, 140.5, 133.5, 129.5 (d, $^3J_{CF}$ = 8.5 Hz), 128.7, 128.3, 116.3 ($^2J_{CF}$ = 21.8 Hz), 20.61, 20.57 ppm. ^{19}F{^{1}H} NMR (376 MHz, CDCl$_3$) δ_F = -111.2 (s). FTIR (solid, cm^{-1}) (ATR) v$_{max}$: 1653 (C=N stretch), 1624 (C=N stretch), 1599, 1535, 1514, 1487, 1441, 1375, 1329, 1315, 1283, 1211, 1161, 1107, 1047, 1020, 1005, 1001, 951, 935, 887, 868, 843, 814, 795, 739, 729, 723, 675, 638, 628, 611, 594, 552, 513, 488, 457, 434, 419. UV-vis (MeCN): λ_{max} ($\varepsilon \times 10^4$ /L mol^{-1} cm^{-1}) 200 (2.9), 258 (3.3), 338 (1.3) nm. HR MS (EI+): *m/z* calc'd 252.1063 for C$_{16}$H$_{13}$FN$_2$; found 252.1063 [M+H]$^+$.

*Synthesis of 6,7-difluoro-2-(4-fluorophenyl)quinoxaline (**LH⁷**)*

As with **LH¹**, but using 2-bromo-4-fluoroacetophenone (1.00 g, 4.61 mmol) and 4,5-difluoro-1,2-phenylenediamine (0.797 g, 1.2 eq, 5.53 mmol). The product was isolated as an off-white solid. Yield = 0.462 g, 39 %. ^{1}H NMR (400 MHz, CDCl$_3$) δ_H = 9.29 (s, 1H), 8.24 – 8.17 (m, 2H), 7.93 – 7.85 (m, 2H), 7.34 – 7.23 (m, 2H) ppm. ^{13}C{^{1}H} NMR (101 MHz, CDCl$_3$) δ_C = 164.6 (d, $^1J_{CF}$ = 251.6 Hz), 154.3 – 153.3 (m), 151.1, 143.2 (d, $^3J_{CF}$ = 3.1 Hz), 140.0 – 138.9 (m), 132.5, 129.7 (d, $^3J_{CF}$ = 8.6 Hz), 116.6 (d, $^2J_{CF}$ = 21.9 Hz), 115.3 (dd, $^2J_{CF}$ = 17.3, $^3J_{CF}$ = 1.7 Hz), 115.1 (dd, $^2J_{CF}$ = 17.4, $^3J_{CF}$ = 2.0 Hz) ppm. ^{19}F{^{1}H} NMR (376 MHz, CDCl$_3$) δ_F = -109.8 (s), -129.2 (d, $^3J_{FF}$ = 21 Hz), -130.1 (d, $^3J_{FF}$ = 21 Hz) ppm. FTIR (solid, cm^{-1}) (ATR) v$_{max}$: 3042, 1632, 1603, 1501, 1441, 1440, 1350, 1310, 1300, 1285, 1223, 1204, 1175, 1155, 1132, 1103, 1040, 1011, 955, 924, 885, 876, 868, 831, 787, 756, 731, 718, 650, 642, 608, 579, 509, 488, 451, 442. UV-vis (MeCN): λ_{max} ($\varepsilon \times 10^4$ /L mol^{-1} cm^{-1}) 202 (3.4), 249 (2.1), 330 (1.2) nm. HR MS (EI+): *m/z* calc'd 261.0640 for C$_{14}$H$_7$F$_3$N$_2$; found 261.0641 [M+H]$^+$.

*Synthesis of 2-(3,4,5-fluorophenyl)quinoxaline (**LH⁸**)*

As with **LH¹**, but using 2-bromo-3,4,5-fluoroacetophenone (1.146 g, 4.530 mmol) and 1,2-phenylenediamine (0.588 g, 1.2 eq, 5.44 mmol). The product was isolated as pale yellow crystals. Yield = 0.500 g, 42 %. ^{1}H NMR (500 MHz, CDCl$_3$) δ 9.24 (s, 1H), 8.18

– 8.09 (m, 2H), 7.92 – 7.85 (m, 2H), 7.84 – 7.77 (m, 2H) ppm. ^{13}C NMR (126 MHz, CDCl$_3$) δ 152.0 (ddd, $^1J_{CF}$ = 250.9, $^2J_{CF}$ = 10.2, $^3J_{CF}$ = 4.0 Hz), 149.5 – 148.3 (m), 141.4 (dt, $^1J_{CF}$ = 256.7, $^2J_{CF}$ = 15.4 Hz), 142.3, 142.1 (d, $^3J_{CF}$ = 5.6 Hz), 132.9 (dd, $^3J_{CF}$ = 7.5, $^4J_{CF}$ = 4.5 Hz), 131.0, 130.6, 129.8, 129.4, 118.8 (dd, $^2J_{CF}$ = 17.1, $^3J_{CF}$ = 5.5 Hz) ppm. ^{19}F NMR (376 MHz, CDCl$_3$) δ$_F$ = -132.6 (d, $^3J_{FF}$ = 20 Hz), -157.5 (t, $^3J_{FF}$ = 20 Hz) ppm. FTIR (solid, cm^{-1}) (ATR) v$_{max}$: 2082, 1532, 1494, 1437, 1420, 1366, 1325, 1248, 1207, 1131, 1055, 1042, 978, 918, 891, 880, 775, 772, 749, 707, 694, 638, 618, 578, 530, 452, 444, 431. UV-vis (MeCN): λ$_{max}$ (ε × 10^4 /L mol^{-1} cm^{-1}) 208 (1.42), 258 (2.5), 333 (1.0) nm. HR MS (ES$^+$): *m/z* calc'd 261.0640 for C$_{14}$H$_7$F$_3$N$_2$; found 261.0647 [M+H]$^+$.

*Synthesis of 6,7-dimethyl-2-(3,4,5-fluorophenyl)quinoxaline (**LH^9**)*

As with **LH^1**, but using 2-bromo-3,4,5-fluoroacetophenone (0.947 g, 3.743 mmol) and 4,5-dimethyl-1,2-phenylenediamine (0.612 g, 1.2 eq, 4.49 mmol). The product was isolated as an off-white solid. Yield = 0.508 g, 47 %. ^{1}H NMR (500 MHz, CDCl$_3$) δ 9.13 (s, 1H), 7.90 – 7.80 (m, 4H), 2.52 (overlapping s, 6H) ppm. ^{13}C{^{1}H} NMR (126 MHz, CDCl$_3$) δ 151.9 (ddd, $^1J_{CF}$ = 250.7, $^2J_{CF}$ = 10.1, $^3J_{CF}$ = 3.8 Hz), 147.7 – 147.5 (m), 141.8 – 141.1 (m), 133.4 – 133.2 (m), 128.8, 128.3, 111.6 (dd, $^2J_{CF}$ = 17.3, $^3J_{CF}$ = 5.5 Hz), 20.6 (overlapping) ppm. ^{19}F{^{1}H} NMR (376 MHz, CDCl$_3$) δ$_F$ = -132.9 (d, $^3J_{FF}$ = 21 Hz), -158.2 (t, $^3J_{FF}$ = 21 Hz) ppm. FTIR (solid, cm^{-1}) (ATR) v$_{max}$: 2091, 1624, 1604, 1528, 1488, 1449, 1444, 1400, 1361, 1332, 1256, 1243, 1203, 1165, 1058, 1046, 1039, 1022, 1002, 979, 893, 887, 875, 764, 737, 705, 697, 643, 638, 558, 492, 463, 463, 458, 442, 434, 420. UV-vis (MeCN): λ$_{max}$ (ε × 10^4 /L mol^{-1} cm^{-1}) 211 (1.3), 263 (3.2), 342 (1.2) nm. HR MS (ES+): *m/z* calc'd 289.0953 for C$_{14}$H$_7$F$_3$N$_2$; found 289.0951 [M+H]$^+$.

*Synthesis of 6,7-difluoro-2-(3,4,5-fluorophenyl)quinoxaline (**LH^{10}**)*

As with **LH^1**, but using 2-bromo-3,4,5-fluoroacetophenone (1.453 g, 5.743 mmol) and 4,5-difluoro-1,2-phenylenediamine (0.993 g, 1.2 eq, 6.891 mmol). The product was isolated as a pale yellow solid. Yield = 0.551 g, 38 %. ^{1}H NMR (500 MHz, CDCl$_3$) δ 9.20 (s, 1H), 7.91 – 7.79 (m, 4H) ppm. ^{13}C NMR (126 MHz, CDCl$_3$) δ 152.0 (ddd, $^1J_{CF}$ = 251.8, $^2J_{CF}$ = 10.2, $^3J_{CF}$ = 4.0 Hz), 153.2 (dd, $^1J_{CF}$ = 256.1, $^2J_{CF}$ = 13.6 Hz), 152.8 (dd, $^1J_{CF}$ = 257.8, $^2J_{CF}$ = 15.4 Hz), 148.9 – 148.5 (m), 141.6 (dt, $^1J_{CF}$ = 257.5, $^2J_{CF}$ = 15.4 Hz), 142.3 (d, $^3J_{CF}$ = 3.2 Hz), 132.3 (td, $^3J_{CF}$ = 7.5, $^4J_{CF}$ = 4.5 Hz), 115.3 (dd, $^2J_{CF}$ =

17.3, $^3J_{CF}$ = 1.8 Hz), 115.1 (dd, $^2J_{CF}$ = 17.4, $^3J_{CF}$ = 1.9 Hz) ppm. $^{19}F\{^1H\}$ NMR (376 MHz, CDCl$_3$) δ_F = -128.1 (d, $^3J_{FF}$ = 21 Hz), -128.5 (d, $^3J_{FF}$ = 21 Hz), -132.3 (d, $^3J_{FF}$ = 21 Hz), -156.7 (dd, $^3J_{FF}$ = 21 Hz) ppm. FTIR (solid, cm^{-1}) (ATR) v_{max}: 2985, 1629, 1606, 1536, 1503, 1484, 1457, 1412, 1379, 1370, 1354, 1259, 1232, 1218, 1211, 1197, 1187, 1167, 1059, 1044, 985, 944, 937, 886, 877, 868, 843, 776, 746, 710, 692, 678, 639, 630, 611, 587, 532, 512, 496, 463, 446, 435. UV-vis (MeCN): λ_{max} ($\varepsilon \times 10^4$/L mol^{-1} cm^{-1}) 208 (2.2), 253 (2.1), 334 (1.2) nm. HR MS (ES+): m/z calc'd 297.0451 for C$_{14}$H$_7$F$_3$N$_2$; found 297.0454 [M+H]$^+$.

Synthesis of the Ir(III) Complexes

Synthesis of Ir(III) μ-chloro bridged dimers:

The chloride-bridged dimer precursors of [(L^n)$_2$Ir(μ-Cl)$_2$Ir(L^n)$_2$] were synthesized by the Nonoyama route.[23] Hydrated IrCl$_3$ and **LH**^{n} (2.0 eq, 0.881 mmol) dissolved in 2-methoxyethanol and distilled water (3:1) (20 mL) and the mixture was heated to reflux under a nitrogen atmosphere whilst stirring for 48 h. The reaction mixture was then cooled to room temperature and precipitates formed upon addition of water (30 mL). The solids were collected by filtration under reduced pressure, washed with water and a small amount of ethanol, to give the crude products as orange solids, which were used in subsequent steps without further purification or characterization.

*Preparation of [Ir(**L¹**)$_2$(bipy)]PF$_6$*

Upon cooling, saturated NH$_4$PF$_6$ solution was added, and the product precipitated as the PF$_6$ salt. The product was purified by silica gel column chromatography (DCM / MeOH, 95:5), collecting the first red band that eluted. The solvent was removed *in vacuo* and then product dissolved in a minimum amount of DCM and recrystallized with diethyl ether. The product was filtered under reduced pressure and dried in an oven overnight to give a red solid. Yield = 0.023 g, 10 %. ^1H NMR (500 MHz, CDCl$_3$) δ_H = 9.36 (s, 2H), 8.53 (d, $^3J_{HH}$ = 6.8 Hz, 2H), 8.10-8.05 (m, 2H), 8.01 (d, $^3J_{HH}$ = 4.9 Hz, 2H), 7.75 (s, 2H), 7.40-7.45 (m, 4H), 6.70 (s, 2H), 6.14 (s, 2H), 2.33 (s, 6H), 2.27 (s, 6H), 1.95 (s, 6H), 1.75 (s, 6H) ppm. $^{13}C\{^1H\}$ NMR (126 MHz, CDCl$_3$) δ_C = 162.2, 155.9, 148.9, 147.9, 143.2, 141.8, 141.4, 140.9, 140.8, 140.5, 140.3, 139.6, 135.1, 131.9, 129.8, 128.7, 127.8, 125.5, 123.0, 20.4, 20.3, 19.8, 19.7 ppm. FTIR (solid, cm$^-$

[1]) (ATR) v_{max}: 1597, 1518, 1447, 1342, 1314, 1281, 1215, 1148, 1074, 1005, 835, 768, 662, 640, 556, 442, 426, 417, 403 cm^{-1}. UV-vis (MeCN): λ_{max} ($\varepsilon \times 10^4$ / L mol^{-1} cm^{-1}) 267 (3.5), 293 (3.1), 378 (1.7), 485 (0.4) nm. HRMS m/z calc'd 871.3100 for C$_{46}$H$_{42}$N$_6$^{193}Ir; found 871.3391 [M − PF$_6$]$^+$.

*Preparation of [Ir(**L^2**)$_2$(bipy)]PF$_6$:*
Prepared as for [Ir(**L^1**)$_2$(bipy)]PF$_6$ but using [(**L^4**)$_2$Ir(μ-Cl)$_2$Ir(**L^4**)$_2$] (0.040 g, 0.026 mmol) and 2,2'-bipyridine (0.009 g, 2.2 eq, 0.057 mmol) to yield a red solid (0.010 g, 19 %). ^{1}H NMR (500 MHz, CDCl$_3$) δ_H 9.46 (s, 2H), 8.52 (d, J = 8.1 Hz, 2H), 8.15 − 8.11 (m, 4H), 8.00 − 7.98 (m, 2H), 7.92 (s, 2H), 7.84 (dd, J = 9.3, 8.3 Hz, 2H), 7.54 (ddd, J = 7.6, 5.5, 1.2 Hz, 2H), 6.73 (dd, J = 11.8, 7.5 Hz, 2H), 6.12 (s, 2H), 2.29 (s, 6H), 1.99 (s, 6H) ppm. ^{19}F{^{1}H} NMR (376 MHz, CDCl$_3$) δ_F -72.6 (d, $^1J_{FP}$ = 711 Hz), -123.8 (d, $^3J_{FF}$ = 22 Hz), -128.6 (d, $^3J_{FF}$ = 22 Hz) ppm. ^{13}C{^{1}H} NMR (101 MHz, (CD$_3$)$_2$CO) δ 156.7, 150.7, 149.7, 145.1, 143.6, 141.8, 141.4, 136.1, 133.0, 130.3, 130.1, 126.0, 111.6, 20.1, 19.5 ppm. UV-vis (MeCN): λ_{max} ($\varepsilon \times 10^4$ / L mol^{-1} cm^{-1}) 266 (3.6), 292 (3.1), 373 (2.1), 518 (0.4) nm. HRMS (EI+): m/z calc'd 885.2074 for C$_{42}$H$_{30}$N$_6$F$_4$^{193}Ir; found 885.2098 [M − PF$_6$]$^+$.

*Preparation of [Ir(**L^5**)$_2$(bipy)]PF$_6$:*
Prepared as for [Ir(**L^1**)$_2$(bipy)]PF$_6$ but using [(**L^5**)$_2$Ir(μ-Cl)$_2$Ir(**L^5**)$_2$] (0.1 g, 0.0743 mmol) and 2,2'-bipyridine (0.029 g, 2.2 eq, 0.16 mmol). Yield = 0.04 g, 34 %. ^{1}H NMR (400 MHz, CD$_3$CN) δ_H = 9.43 (s, 2H), 8.39 (d, J = 8.4 Hz, 2H), 8.13 (dd, J = 8.7, 5.4 Hz, 2H), 8.01 (dd, J = 8.1, 4.8 Hz, 2H), 7.94 (d, J = 5.7 Hz, 2H), 7.56 (app. t, J = 7.8 Hz, 2H), 7.45 − 7.40 (m, 2H), 7.13 (d, J = 4.9 Hz, 2H), 7.13 − 7.08 (m, 2H), 6.92 (dd, J = 9.8, 7.3 Hz, 2H), 6.88 (d, J = 9.3 Hz, 2H), 5.98 (dd, J = 9.0, 2.3 Hz, 2H) ppm. ^{19}F{^{1}H} NMR (376 MHz, CDCl$_3$) δ_F = -73.4 (d, $^1J_{FP}$ = 720 Hz), -103.6 (s) ppm. UV-vis (MeCN): λ_{max} ($\varepsilon \times 10^4$ / L mol^{-1} cm^{-1}) 460 sh (0.2), 359 (0.7), 288 (2.4), 249 (2.7). HR MS (EI+): m/z calc'd 793.1636 for C$_{38}$H$_{24}$N$_6$F$_2$^{193}Ir; found 793.1649 [M − PF$_6$]$^+$.

*Preparation of [Ir(**L^6**)$_2$(bipy)]PF$_6$:*
Prepared as for [Ir(**L^1**)$_2$(bipy)]PF$_6$ but using [(**L^6**)$_2$Ir(μ-Cl)$_2$Ir(**L^6**)$_2$] (0.320 g, 0.219 mmol) and 2,2'-bipyridine (0.075 g, 2.2 eq, 0.482 mmol). Yield = 0.027 g, 16 %. ^{1}H NMR (400 MHz, CD$_3$CN) δ_H = 9.50 (s, 2H), 8.32 (dd, $^3J_{HF}$ = 8.7, $^3J_{HH}$ 5.6 Hz, 2H), 8.25 (d, $^3J_{HH}$ =

8.2 Hz, 2H), 8.15 (d, $^3J_{HH}$ = 5.7 Hz, 2H), 8.02 – 8.07 (m, 2H), 7.79 (s, 2H), 7.53 – 7.58 (m, 2H), 7.05 – 6.99 (m, 2H), 6.78 (s, 2H), 6.21 – 6.16 (m, 2H), 2.31 (s, 6H), 1.76 (s, 6H) ppm. $^{13}C\{^1H\}$ NMR (101 MHz, CD$_3$CN) δ_C = 156.5, 150.4, 143.8, 142.2, 142.0, 141.2, 130.6, 130.0, 125.6, 124.0, 20.3, 19.7 ppm. $^{19}F\{^1H\}$ NMR (376 MHz, CDCl$_3$) δ_F = -73.6 (d, $^1J_{FP}$ = 720 Hz), -104.9 (s) ppm. FTIR (solid, cm^{-1}) (ATR) v_{max}: 1587, 1566, 1526, 1445, 1341, 1258, 1196, 1123, 1065, 851, 810, 775, 735, 656, 557, 459, 446, 409. UV-vis (MeCN): λ_{max} ($\varepsilon \times 10^4$ / L mol^{-1} cm^{-1}) 286 (4.9), 372 (2.4), 450 (0.7) nm. HR MS (EI+): *m/z* calc'd 849.2263 for C$_{42}$H$_{32}$N$_6$F$_2$^{193}Ir; found 849.2287 [M – PF$_6$]$^+$.

*Preparation of [Ir(**L^7**)$_2$(bipy)]PF$_6$:*
Prepared as for [Ir(**L^1**)$_2$(bipy)]PF$_6$ but using [(**L^7**)$_2$Ir(μ-Cl)$_2$Ir(**L^7**)$_2$] (0.093 g, 0.062 mmol) and 2,2'-bipyridine (0.021 g, 2.2 eq, 0.014 mmol). Yield = 0.026 g, 21 %. ^1H NMR (500 MHz, CD$_3$CN) δ 9.59 (s, 2H), 8.38 (dd, J = 8.8, 5.6 Hz, 2H), 8.28 (d, J = 8.1 Hz, 2H), 8.13 – 8.03 (m, 4H), 7.94 (dd, J = 10.3, 8.4 Hz, 2H), 7.56 (dd, J = 7.1, 6.0 Hz, 2H), 7.12 – 6.98 (m, 2H), 6.80 (dd, J = 12.4, 7.8 Hz, 2H), 6.28 (dd, J = 9.5, 2.5 Hz, 2H) ppm. $^{13}C\{^1H\}$ NMR (101 MHz, CD$_3$CN) δ_C = 165.7 (d, $^1J_{CF}$ = 257.5 Hz), 164.4 (d, $^3J_{CF}$ = 2.6 Hz), 156.8, 156.1 (d, $^2J_{CF}$ = 7.3 Hz), 150.3, 145.6 (d, $^3J_{CF}$ = 3.1 Hz), 141.7, 141.0 (d, $^3J_{CF}$ = 1.0 Hz), 140.9, 140.0 – 139.2 (m), 132.6, 132.5, 130.5, 126.5, 121.8 (d, $^2J_{CF}$ = 19.0 Hz), 112.8 (d, $^2J_{CF}$ = 23.7 Hz), 112.12 (d, $^2J_{CF}$ = 22.7 Hz) ppm. ^{19}F NMR (376 MHz, CD$_3$CN) δ -73.0 (d, $^1J_{FP}$ = 720 Hz), -106.5 (s), -128.57 (d, $^3J_{FF}$ = 22 Hz), -133.1 (d, $^3J_{FF}$ = 22 Hz) ppm. FTIR (solid, cm^{-1}) (ATR) v_{max}: 1588, 1570, 1534, 1509, 1448, 1353, 1262, 1232, 1202, 1165, 1126, 1065, 1031, 835, 817, 765, 738, 669, 628, 556, 447, 418. UV-vis (MeCN): λ_{max} ($\varepsilon \times 10^4$ / L mol^{-1} cm^{-1}) 206 (4.8), 259 (2.9), 284 (2.5), 362 (1.6), 449 (0.4) nm. HR MS (ES+): *m/z* calc'd 867.1283 for C$_{38}$H$_{20}$N$_6$F$_6$^{193}Ir; found 867.1292 [M – PF$_6$]$^+$.

*Preparation of [Ir(**L^8**)$_2$(bipy)]PF$_6$:*
Prepared as for [Ir(**L^1**)$_2$(bipy)]PF$_6$ but using [(**L^8**)$_2$Ir(μ-Cl)$_2$Ir(**L^8**)$_2$] (0.216 g, 0.145 mmol) and 2,2'-bipyridine (0.050 g, 2.2 eq, 0.319 mmol). Yield = 0.054 g, 37 %. ^1H NMR (500 MHz, (CD$_3$)$_2$CO) δ_H = 9.74 (s, 2H), 8.53 (dd, $^3J_{HH}$ = 5.6, $^4J_{HH}$ 0.8 Hz, 2H), 8.45 (ddd, J = 10.8, 6.6, 1.6 Hz, 2H), 8.33 (d, J = 8.1 Hz, 2H), 8.20 – 8.10 (m, 2H), 7.92 (dd, J = 8.3, 1.1 Hz, 2H), 7.75-7.65 (m, 2H), 7.58 (ddd, J = 7.6, 5.6, 1.3 Hz, 2H), 7.20 – 7.10 (m, 4H) ppm. $^{19}F\{^1H\}$ NMR (376 MHz, CDCl$_3$) δ_F = -73.0 (d, $^1J_{FP}$ = 720 Hz), -127.1 (dd,

J_{FF} = 22, 6 Hz), -142.2 (dd, J_{FF} = 22, 6 Hz), -156.0 – -156.2 (m) ppm. FTIR (solid, cm^{-1}) (ATR) v_{max} : 1705, 1628, 1604, 1539, 1478, 1469, 1417, 1367, 1298, 1200, 1141, 1137, 1045, 830, 677, 737, 674, 639, 556. UV-vis (MeCN): λ_{max} ($\varepsilon \times 10^4$ /L mol^{-1} cm^{-1}) 208 (2.4), 241 (1.8), 283 (1.9), 357 (1.1), 370 (1.1), 442 (0.2) nm. HR MS (ES+): *m/z* calc'd 867.1283 for $C_{38}H_{20}N_6F_6{}^{193}Ir$; found 867.1296 [M – PF$_6$]$^+$.

*Preparation of [Ir(**L^9**)$_2$(bipy)]PF$_6$:*

Prepared as for [Ir(**L^1**)$_2$(bipy)]PF$_6$ but using [(**L^9**)$_2$Ir(μ-Cl)$_2$Ir(**L^9**)$_2$] (0.067 g, 0.042 mmol) and 2,2'-bipyridine (0.014 g, 2.2 eq, 0.092 mmol). Yield = 0.013 g, 28 %. ^{1}H NMR (500 MHz, CD$_3$CN) δ_H = 9.31 (s, 2H), 8.22 (dd, $^3J_{HH}$ = 5.6, $^4J_{HH}$ = 0.8 Hz, 2H), 8.08 (ddd, *J* = 10.8, 6.6, 1.6 Hz, 2H), 8.03 (d, *J* = 8.0 Hz, 2H), 7.94 – 7.89 (m, 2H), 7.63 (s, 2H), 7.49 (ddd, *J* = 7.6, 5.6, 1.3 Hz, 2H), 6.69 (s, 2H), 2.17 (s, 3H), 1.67 (s, 3H) ppm. ^{13}C NMR (126 MHz, CD$_3$CN) δ 161.6, 156.4, 150.0, 144.6, 143.4, 142.7, 141.9, 141.7, 141.1, 130.1, 130.1, 125.6, 124.2, 113.8 (dd, $^2J_{CF}$ = 18.8, $^3J_{CF}$ = 3.2 Hz), 113.3, 113.2, 20.1, 19.6 ppm. ^{19}F{^{1}H} NMR (376 MHz, CD$_3$CN) δ_F = -127.3 (dd, $^3J_{FF}$ = 22.0, $^4J_{FF}$ 5.5 Hz), -142.7 (dd, $^3J_{FF}$ = 18.9, $^4J_{FF}$ = 5.5 Hz), -157.0 (dd, $^3J_{FF}$ = 21.9, 19.0 Hz) ppm. FTIR (solid, cm^{-1}) (ATR) v_{max} : 1559, 1533, 1481, 1466, 1437, 1369, 1297, 1163, 1045, 1026, 911, 855, 850, 796, 780, 738, 704, 672, 556, 520, 484, 453. UV-vis (MeCN): λ_{max} ($\varepsilon \times 10^4$ / L mol^{-1} cm^{-1}) 239 (4.3), 284 (4.6), 363 (2.2), 379 (2.9), 439 (0.7) nm. HR MS (ES+): *m/z* calc'd 923.1909 for $C_{42}H_{28}N_6F_6{}^{193}Ir$; found 923.1918 [M – PF$_6$]$^+$.

*Preparation of [Ir(**L^{10}**)$_2$(bipy)]PF$_6$:*

Prepared as for [Ir(**L^1**)$_2$(bipy)]PF$_6$ but using [(**L^{10}**)$_2$Ir(μ-Cl)$_2$Ir(**L^{10}**)$_2$] (0.069 g, 0.422 mmol) and 2,2'-bipyridine (0.014 g, 2.2 eq, 0.093 mmol). Yield = 0.015 g, 34 %. ^{1}H NMR (500 MHz, (CD$_3$)$_2$CO) δ 9.78 (s, 2H), 8.57 (dd, *J* = 5.6, 0.8 Hz, 2H), 8.55 – 8.45 (m, 4H), 8.22 – 8.15 (m, 2H), 7.93 (dd, *J* = 10.2, 8.4 Hz, 2H), 7.73 (ddd, *J* = 7.6, 5.6, 1.3 Hz, 2H), 6.98 (dd, *J* = 12.2, 7.7 Hz, 2H) ppm. ^{19}F{^{1}H} NMR (376 MHz, (CD$_3$)$_2$CO) δ_F = -72.5 (d, $^1J_{FP}$ = 740 Hz), -126.93 (dd, $^3J_{FF}$ = 22.3, $^4J_{FF}$ = 5.7 Hz), -127.86 (d, $^3J_{FF}$ = 21.7 Hz), -131.44 (d, $^3J_{FF}$ = 21.7 Hz), -141.70 (dd, $^3J_{FF}$ = 19.2, $^4J_{FF}$ = 5.7 Hz), -154.43 – -155.35 (m) ppm. FTIR (solid, cm^{-1}) (ATR) v_{max}: 2945, 1732, 1541, 1495, 1470, 1443, 1404, 1373, 1250, 1234, 1202, 1165, 1045, 1007, 837, 766, 673, 625, 557, 442, 419. UV-vis (MeCN): λ_{max} ($\varepsilon \times 10^4$ / L mol^{-1} cm^{-1}) 208 (2.7), 239 (1.8), 280 (1.6), 360 (1.0), 372 (1.0), 440 (0.2) nm. HR MS (ES+): *m/z* calc'd 939.0906 for $C_{38}H_{16}N_6F_{10}{}^{193}Ir$; found 939.0911 [M – PF$_6$]$^+$.

Associated Content

CCDC2090298-2090301 contains supplementary X-ray crystallographic data for [Ir(**L^1**)$_2$(bipy)]PF$_6$, [Ir(**L^2**)$_2$(bipy)]PF$_6$, [Ir(**L^5**)$_2$(bipy)]PF$_6$ and [Ir(**L^6**)$_2$(bipy)]PF$_6$ respectively. This data can be obtained free of charge via http://www.ccdc.cam.ac.uk/conts/retrieving.html, or from the Cambridge Crystallographic Data Centre, Union Road, Cambridge, CB2 1EZ; fax(+44) 1223-336-033 or email: deposit@ccdc.cam.ac.uk.

Author Information

Corresponding Author

E-mail: popesj@cardiff.ac.uk

ORCID

Present Address

S.J.A.P.: School of Chemistry, Main Building, Cardiff University, Wales, UK CF10 3AT.

Notes

The authors declare no competing financial interest.

Supporting Information

Data collection parameters, tabulated bond lengths and bond angles for the X-ray crystallography; additional figures to support the discussion of the spectroscopic properties of the complexes; additional figures and tables to support discussion of the DFT calculations.

References

(1) Renault, J.; Giorgi-Renault, S.; Mailliet, P.; Baron, M.; Paoletti, C.; Cros, S. Heterocyclic quinones 2. Quinoxaline-5,6-(and 5-8)-diones – potential anti-tumoral agents *Eur. J. Med. Chem.* **1981**, *16*, 545

(2) Pereira, J.A.; Pessoa, A.M.; Natalia M.; Cordeiro, D.S.; Fernandes, R.; Prudencio, C.; Noronha, J.P.; Vieira, M. Quinoxaline, its derivatives and applications: a state of the art review *Eur. J. Med. Chem.* **2015**, *97*, 664.

(3) Yuan, J.; Ouyang, J.; Cimrová, V.; Leclerc, M.; Najarid, A.; Zou, Y. Development of quinoxaline based polymers for photovoltaic applications *J. Mat Chem*. C **2017**, *5*, 1858.

(4) Wu, X.; Gorden, A.E.V.; Tonks, S.A.; Vilseck, J.Z. Regioselective synthesis of asymmetrically substituted 2-quinoxalinol salen ligands *J. Org. Chem.* **2007**, *72*, 8691

(5) For example, (a) Dhanaraj, C.J.; Johnson, J. Studies on some metal complexes of quinoxaline based unsymmetric ligand: synthesis, spectral characterisation, in vitro biological and molecular modelling studies *J. Photochem. Photobiol. B* **2016**, *161*, 108; (b) Dhanaraj, C.J.; Johnson, J.; Joseph, J.; Joseyphus, R.S. Quinoxaline based Schiff base transition metal complexes: review *J. Coord. Chem.* **2013**, *66*, 1416; (c) Cummings, S.D.; Eisenberg, R. Luminescent platinum(II) complexes of quinoxaline-2,3-dithiolate *Inorg. Chem.* **1995**, *34*, 2007; (d) Zhang, S-M.; Hu, T-L.; Li, J-R.; Du, J-L.; Bu, X-H. Silver(I) coordination architectures with quinoxaline-based N,S-donor ligands: structures and luminescent properties *CrystEngComm* **2008**, *10*, 1595; (e) Andrews, M.; Laye, R.H.; Harding, L.P.; Pope, S.J.A. Quinoxaline sensitised lanthanide ion luminescence: Syntheses, spectroscopy and X-ray crystal structure of Na{1,4,7-tris[(N-diethyl)carbamoylmethyl]-1,4,7,10-tetraazacyclododecane -10-(2-methylquinoxaline)}I-3 C7H8 *Polyhedron* **2008**, *27*, 2365.

(6) Clark, A. M.; Rickard, C. E. F.; Roper, W.R.; Wright, L.J. Bromination and nitration reactions of metalated (Ru and Os) multiaromatic ligands and crystal structures of selected products *J. Organomet. Chem.* **2000**, *598*, 262

(7) Guo, B-B.; Azam, M.; Al Resayes, S.I.; Lin, Y.-J.; Jin, G-X. Discrete supramolecular stacks based on multinuclear tweezer-type rhodium complexes *Chem. Eur. J.* **2020**, *26*, 558.

(8) (a) Hwang, F-M.; Chen, H-Y.; Chen, P-S.; Liu, C-S.; Chi, Y.; Shu, C-F.; Wu, F.; Chou, P-T.; Peng, S-M.; Lee, G-H. Iridium(III) complexes with orthometalated quinoxaline ligands: subtle tuning of emission to the saturated red color *Inorg. Chem.* **2005**, *44*, 1344; (b) Sengottuvelan, N.; Yun, Seong-Jae; Kim, D-Y.; Hwang, I-H.; Kang, S. K.; Kim, Y-I. Highly efficient red emissive heteroleptic cyclometalated iridium(III) complexes bearing two substituted 2-phenylquinoxaline and one 2-pyrazinecarboxylic acid *Bull. Kor. Chem. Soc.* **2013**, *34*, 167; (c) Sengottuvelan, N.; Yun, S-J.; Kang, S. K.; Kim, Y-I. Red-Orange Emissive Cyclometalated Neutral Iridium(III) Complexes and Hydridoiridium(III) Complex Based on 2-Phenylquinoxaline: Structure, Photophysics and Reactivity of Acetylacetone Towards Cyclometalated Iridium Dimer *Bull. Kor. Chem. Soc.* **2011**, *32*, 4321; (d) Sengottuvelan, N.; Seo, H-J.; Kang, S.K.; Kim, Y-I. Tuning Photophysical and Electrochemical Properties of Heteroleptic Cationic Iridium(III) Complexes Containing Substituted 2-Phenylquinoxaline and Biimidazole *Bull. Kor. Chem. Soc.* **2010**, *31*, 2309.

(9) Culham, S.; Lanoe, P-H.; Whittle, V. L.; Durrant, M. C.; Williams, J. A. G.; Kozhevnikov, V.N. Highly luminescent dinuclear platinum(II) complexes incorporating bis-cyclometallating pyrazine-based ligands: a versatile approach to efficient red phosphors *Inorg. Chem.* **2013**, *52*, 10992.

(10) For general overviews see: (a) *Iridium(III) in Optoelectronic and Photonics Applications* Ed. Zysman-Colman, E. Wiley, 2017; (b) Ma, D-K.; Lin, S.; Wang, W.; Yang, C.; Leung, C-H. Luminescent chemosensors by using cyclometalated iridium(III) complexes and their applications *Chem. Sci.* **2017**, *8*, 878; (c) Zhao, Q.; Huang, C.; Li, F. Phosphorescent heavy-metal complexes for bioimaging *Chem. Soc. Rev.* **2011**, *40*, 2508; (d) Ma, D-L.; Ma, V. P-Y.; Chan, D.S-H.; Leung, K-H.; He, H-Z.; Leung, C-H. Recent advances in luminescent heavy metal complexes for sensing *Coord. Chem. Rev.* **2012**, *256*, 3087; (e) Caporale, C.; Massi, M. Cyclometalated iridium(III) complexes for life science *Coord. Chem. Rev.* **2018**, *363*, 71; (f) Lo, K.K.; Louie, M-W.; Zhang, K. *Coord. Chem. Rev.* Design of luminescent iridium(III) and rhenium(I) polypyridine complexes as in vitro and in vivo ion, molecular and biological probes **2010**, *254*, 2603; (g) Zamora, A.; Vigueras, G.; Rodrgiguez, V.; Santana, M.D.; Ruiz, J. Cyclometalated iridium(III) luminescent complexes in therapy and phototherapy *Coord. Chem. Rev.* **2018**, *360*, 34; (h) Williams, J. A. G. The coordination chemistry of dipyridylbenzene: N-deficient terpyridine or panacea for brightly luminescent metal complexes? *Chem. Soc. Rev.* **2009**, *38*, 1783; (i) Ladouceur, S.;

Zysman-Colman, A comprehensive survey of cationic iridium(III) complexes bearing nontraditional ligand chelation motifs E. *Eur. J Inorg. Chem.* **2013**, 2985; (j) Mills, I.N.; Porras, J.A.; Bernhard, S. Judicious choice of cationic cyclometalated Ir(III) complexes for photochemical energy conversion and optoelectronics*, Acc. Chem. Res.* **2018**, *51*, 352; (k) Zanoni, K.P.S.; Coppo, R.L.; Amaral, R.C.; Iha, N.Y.M. Ir(III) complexes designed for light-emitting devices: beyond the luminescence color array, *Dalton Trans.* **2015**, *44*, 14559; (l) Pal, A.K.; Cordes, D.B.; Slawin, A.M.Z.; Moblona, C.; Orti, E.; Samuel, I.D.W.; Bolink, H.J.; Zysman-Colman, E. Synthesis, properties, and light-emitting electrochemical cell device fabrication of cationic Ir(III) complexes bearing electron-withdrawing groups on the cyclometallating ligands, *Inorg. Chem.* **2016**, *55*, 10361.

(11) DiLuzio, S.; Mdluli, V.; Connell, T.U.; Lewis, J.; VanBenschoten, V.; Bernhard, S. High-throughput screening and automated data-driven analysis of the triplet photophysical properties of structurally diverse, heteroleptic iridium(III) complexes *J. Am. Chem. Soc.* **2021**, *143*, 1179.

(12) Groves, L.M.; Schotten, C.; Beames, J.M.; Platts, J.A.; Coles, S.J.; Horton, P.N.; Browne, D.L.; Pope, S.J.A. From ligand to phosphor: rapid, machine-assisted synthesis of substituted iridium(III) pyrazolate complexes with tuneable luminescence *Chem. Eur. J.* **2017**, *23*, 9407

(13) (a) Monos, T.M.; Sun, A.C.; McAtee, R.C.; Devery, J.J.; Stephenson, C.R.J. Microwave assisted synthesis of heteroleptic Ir(III) polypyridyl complexes *J. Org. Chem.* **2016**, *81*, 6988; (b) Davies, D.L.; Lowe, M.P.; Ryder, K.S.; Singh, K.; Singh, S. Tuning emission wavelength and redox properties through position of the substituent in iridium(III) cyclometallated complexes *Dalton Trans.* **2011**, *40*, 1028; (c) Alam, P.; Laskar, I.R.; Climent, C.; Casanova, D.; Alemany, P.; Karanam, M.; Choudhury, A.R.; Butcher, J.R. Microwave-assisted facile and expeditive syntheses of phosphorescent cyclometallated iridium(III) complexes *Polyhedron* **2013**, *53*, 286; (d) Wu, Q-H.; Wang, C-H.; Song, X-M.; Zhang, G-L. Microwave-assisted synthesis of a new triplet iridium(III) pyrazine complex *Chin. J. Chem. Phys.* **2010**, *23*, 355; (e) Saito, K.; Matsusue, N.; Kanno, H.; Hamada, Y.; Takahashi, H.; Matsumura, T. Microwave synthesis of iridium(III) complexes: synthesis of highly efficient orange emitters in organic light-emitting devices *Jpn. J. Appl. Phys.* **2004**, *43*, 2733; (f) Konno, H. *Chem. Lett.* **2003**, *32*, 252; (g) Constable, E.C.; Housecroft, C.E.; Schönhofer, E.; Schönle,

J.; Zampese, J.A. Softening the donor set for light-emitting electrochemical cells: [Ir(ppy)$_2$(N^N)]$^+$, [Ir(ppy)$_2$(P^P)]$^+$ and [Ir(ppy)$_2$(P^S)]$^+$ salts *Polyhedron* **2012**, *35*, 154.

(14) Vella, J.H.; Parthasarathy, A.; Schanze, K.S. Triplet Sensitization in an Anionic Poly(phenyleneethynylene) Conjugated Polyelectrolyte by Cationic Iridium Complexes *J. Phys. Chem. A* **2013**, *117*, 7818.

(15) (a) Zhou, L.; Wei, F.; Xiang, J.; Li, H.; Li, C.; Zhang, P.; Liu, C.; Gong, P.; Cai, L.; Wong, K. M-C. Enhancing the ROS generation ability of a rhodamine-decorated iridium(iii) complex by ligand regulation for endoplasmic reticulum-targeted photodynamic therapy *Chem. Sci.* **2020**, *11*, 12212; (b) Wang, C.; Lystrom, L.; Yin, H.; Hetu, M.; Kilina, S.; McFarland, S. A.; Sun, W. Increasing the triplet lifetime and extending the ground-state absorption of biscyclometalated Ir(III) complexes for reverse saturable absorption and photodynamic therapy applications *Dalton Trans.* **2016**, *45*, 16366.

(16) (a) You, C.; Liu, D.; Yu, J.; Tan, H.; Zhu, M.; Zhang, B.; Liu, Y.; Wang, Y.; Zhu, W.
Boosting Efficiency of Near-Infrared Emitting Iridium(III) Phosphors by Administrating Their pi-pi Conjugation Effect of Core-Shell Structure in Solution-Processed OLEDs *Adv. Opt. Mat.* **2020**, *8*, 2000154; (b) You, C.; Liu, D.; Meng, F.; Wang, Y.; Yu, J.; Wang, S.; Su, S.; Zhu, W. Iridium(iii) phosphors with rigid fused-heterocyclic chelating architectures for efficient deep-red/near-infrared emissions in polymer light-emitting diodes *J. Mat Chem. C* **2019**, *7*, 10961; (c) Phillips, K.A.; Stonelake, T.M.; Horton, P.N.; Coles, S.J.; Hallett, A.J.; O'Kell, S.P.; Beames, J.M.; Pope, S.J.A. Dual visible/NIR emission from organometallic iridium(III) complexes *J. Organomet. Chem.* **2019**, *893*, 11; (d) Chen, G-Y.; Chang, B-R.; Shih, T-A.; Lin, C-H.; Lo, C-L.; Chen, Y-Z.; Liu, Y-X.; Li, Y-R.; Guo, J-T.; Lu, C-W.; Yang, Z-P.; Su, H-C. Cationic Ir(III) Emitters with Near-Infrared Emission Beyond 800 nm and Their Use in Light-Emitting Electrochemical Cells *Chem. Eur. J.* **2019**, *25*, 5489; (e) Guo, J.; Zhou, J.; Guorui, F.; He, Y.; Li, W.; Lu, X. Two efficient near-infrared (NIR) luminescent [Ir(CN)(2)(NO)]-characteristic complexes with 8-hydroxyquinoline (8-Hq) as the ancillary ligand *Inorg. Chem. Commun.* **2019**, *101*, 69; (f) Kim, Y-I.; Yun, S-J.; Kim, D.; Kang, S. K. Structural and Photoluminescent Properties of Near-Infrared Emissive Bis(2,3-Diphenylbenzoquinoxalinato)(2-Pyrazinecarboxylato)iridium(III) *Bull. Kor. Chem. Soc.* **2018**, *39*, 133; (g) Jing, Y-M.; Zheng, Y-X. Photoluminescence and electroluminescence of deep red iridium(iii) complexes with 2,3-diphenylquinoxaline

derivatives and 1,3,4-oxadiazole derivatives ligands *RSC Adv.* **2017**, *7*, 37021; (h) Cao, X.; Miao, J.; Zhu, M.; Zhong, C.; Yang, C.; Wu, H.; Qin, J.; Cao, Y. Near-Infrared Polymer Light-Emitting Diodes with High Efficiency and Low Efficiency Roll-off by Using Solution-Processed Iridium(III) Phosphors *Chem. Mater.* **2015**, *27*, 96; (i) Wiegmann, B.; Jones, P.G.; Wagenblast, G.; Lennartz, C.; Muenster, I.; Metz, S.; Kowalsky, W.; Johannes, H-H. A New Framework of a Heteroleptic Iridium(III)-Carbene Complex as a Triplet Emitting Material *Organometallics* **2012**, *31*, 5223; (j) Wang, C.; Wong, K. M-C. Bichromophoric Rhodamine-Iridium(III) Sensory System: Modulation of the Energy-Transfer Process through a Selective Sensing Behavior *Inorg. Chem.* **2011**, *50*, 5333; (k) Ahn, S. Y.; Lee, H. S.; Seo, J-H.; Kim, Y. K.; Ha, Y. Color tuning of red phosphorescence: New iridium complexes containing fluorinated 2,3-diphenylquinoxaline ligands *Thin Sol. Films* **2009**, *517*, 4111.

(17) (a) Wu, W.; Zhang, C.; Rees, T.W.; Liao, X.; Yan, X.; Chen, Y.; Ji, L.; Chao, H. Lysosome-Targeting Iridium(III) Probe with Near-Infrared Emission for the Visualization of NO/O-2(center dot-) Crosstalk via In Vivo Peroxynitrite Imaging *Anal. Chem.* **2020**, *92*, 6003; (b) Chen, Q.; Jin, C.; Shao, X.; Guan, R.; Tian, Z.; Wang, C.; Liu, F.; Ling, P.; Guan, J-L.; Ji, L.; Wang, F.; Chao, H.; Diao, J. Super-Resolution Tracking of Mitochondrial Dynamics with An Iridium(III) Luminophore *Small* **2018**, *14*, e1802166; (c) Jing, Y.; Cao, Q.; Hao, L.; Yang, G-G.; Hu, W-L.; Ji, L-N.; Mao, Z-W. *Chem. Commun.* **2018**, *54*, 271; (d) Jin, C.; Guan, R.; Wu, J.; Yuan, B.; Wang, L.; Huang, J.; Wang, H.; Ji, L.; Chao, H. A self-assessed photosensitizer: inducing and dual-modal phosphorescence imaging of mitochondria oxidative stress *Chem. Commun.* **2017**, *53*, 10374; (e) Wang, L.; Yin, H.; Cui, P.; Hetu, M.; Wang, C.; Monro, S.; Schaller, R. D.; Cameron, C.G.; Liu, B.; Kilina, S.; McFarland, S.A.; Sun, W. Near-infrared-emitting heteroleptic cationic iridium complexes derived from 2,3-diphenylbenzo[g]quinoxaline as in vitro theranostic photodynamic therapy agents *Dalton Trans.* **2017**, *46*, 8091.

(18) Hao, Z.; Zhang, K.; Wang, P.; Lu, X.; Lu, Z.; Zhu, W.; Liu, Y. Deep Red Iridium(III) Complexes Based on Pyrene-Substituted Quinoxaline Ligands for Solution-Processed Phosphorescent Organic Light-Emitting Diodes *Inorg. Chem.* **2020**, *59*, 332.

(19) Matteucci, E.; Baschieri, A.; Mazzanti, A.; Sambri, L.; Avila, J.; Pertegas, A.; Bolink, H.J.; Monti, F.; Leoni, E.; Armaroli, N. Anionic Cyclometalated Iridium(III) Complexes with a Bis-Tetrazolate Ancillary Ligand for Light-Emitting Electrochemical Cells *Inorg. Chem.* **2017**, *56*, 10584.

(20) Langdon-Jones, E.E.; Hallett, A.J.; Routledge, J.D.; Crole, D.A.; Ward, B.D.; Platts, J.A.; Pope, S.J.A. Using substituted cyclometalated quinoxaline ligands to finely tune the luminescence properties of iridium(III) complexes *Inorg. Chem.* **2013**, *52*, 448.

(21) (a) Phillips, K.A.; Stonelake, T.M.; Chen, K.; Hou, Y.; Zhao, J.; Coles, S.J.; Horton, P.N.; Keane, S.J.; Stokes, E.C.; Fallis, I.A.; Hallett, A.J.; O'Kell, S.P.; Beames, J.B.; Pope, S.J.A. Ligand tuneable, red-emitting iridium(III) complexes for efficient triplet-triplet annihilation upconversion performance *Chem. Eur. J.* **2018**, 24, 8577; (b) Elgar, C.E.; Otaif, H.Y.; Zhang, X.;, Zhao, J.; Beames, J.M.; Horton, P.N.; Coles, S.J.; Pope, S.J.A. Iridium(III) sensitizers and energy upconversion: the influence of ligand structure upon TTA-UC performance *Chem. Eur. J.* **2021**, *27*, 3427.

(22) Day, A.H.; Übler, M.H.; Best, H.L.; Lloyd-Evans, E.; Mart, R.J.; Fallis, I. A.; Allemann, R.K.; Al-Wattar, E.A. H.; Keymer, N.I.; Buurma, N.J.; Pope, S.J.A. Targeted cell imaging properties of a deep red luminescent iridium(III) complex conjugated with a c-Myc signal peptide *Chem. Sci.* **2020**, *11*, 1599.

(23) (a) Zhang, R. ; Qin, Y.; Zhang, L.; Luo, S. Oxidative Synthesis of Benzimidazoles, Quinoxalines, and Benzoxazoles from Primary Amines by ortho-Quinone Catalysis *Org. Lett.* **2017**, *19*, 5629; (b) Shee, S.; Panja, D.; Kundu, S. Nickel-Catalyzed Direct Synthesis of Quinoxalines from 2-Nitroanilines and Vicinal Diols: Identifying Nature of the Active Catalyst *J. Org. Chem.* **2020**, *85*, 2775; (c) Qi, C.; Jiang, H.; Huang, L.; Chen, Z.; Chen, H. DABCO-Catalyzed Oxidation of Deoxybenzoins to Benzils with Air and One-Pot Synthesis of Quinoxalines *Synthesis* **2011**, 387; (d) Yuan, H.; Li, K.; Chen, Y.; Wang, Y.; Cui, J.; Chen, B. One-Pot Copper-Catalyzed Three-Component Synthesis of Quinoxalines by Condensation and C-N Bond Formation *Synlett*, **2013**, *24*, 2315; (e) Chen, T.; Chen, X.; Wei, J.; Lin, D.; Xie, Y.; Zeng, W. Copper-Catalyzed Cascade Cycloamination of alpha-Csp(3)-H Bond of N-Aryl Ketimines with Azides: Access to Quinoxalines *Org. Lett.* **2016**, *18*, 2078; (f) Shen, J.; Wang, X.; , X.; Yang, Z.; Cheng, G.; Cui, X. One-Pot Regiospecific Synthesis of via a CH2-Extrusion Reaction *Org. Lett.* **2016**, *18*, 1378; (g) Cho, Y.-H.; Kim, K.-H.; Cheon, C.-H. Synthesis of 2-Aminoquinoxalines via One-Pot Cyanide-Based Sequential Reaction under Aerobic Oxidation Conditions *J. Org. Chem.* **2014**, *79*, 901; (h) Bandaru, S. S. M.; Bhilare, S.; Chrysochos, N.; Gayakhe, V.; Trentin, I.; Schulzke, C.; Kapdi, A. R. Pd/PTABS: Catalyst for Room Temperature Amination of Heteroarenes *Org. Lett.* **2018**, *20*, 473.

(24) Chaudhuri, S.K.; Roy, S.; Bhar, S. Dioxane dibromide mediated bromination of substituted coumarins under solvent-free conditions *Beilstein J. Org. Chem.* **2012**, *8*, 323.

(25) (a) Chen, T.; Chen, X.; Wei, J.; Lin, D.; Xie, Y.; Zeng, W. Copper-Catalyzed Cascade Cycloamination of alpha-Csp(3)-H Bond of N-Aryl Ketimines with Azides: Access to Quinoxalines *Org. Lett.* **2016**, *18*, 2078; (b) Singh, S.K.; Gupta, P.; Duggineni, S.; Kundu, B. Solid phase synthesis of quinoxalines *Synlett* **2003**, *14*, 2147.

(26) Martin, L.J.; Marzinzik, A.L.; Ley, S.V.; Baxendale, I.R. Safe and Reliable Synthesis of Diazoketones and Quinoxalines in a Continuous Flow Reactor *Org. Lett.* **2011**, *13*, 320.

(27) (a) Chen, Y.; Liu, C.; Wang, L. Effects of fluorine substituent on properties of cyclometalated iridium(III) complexes with a 2,2 '-bipyridine ancillary ligand *Tetrahedron* **2019**, *75*, 130686; (b) Sun, P.; Wang, K.; Zhao, B.; Yang, T.; Xu, H.; Miao, Y.; Wang, H.; Xu, B. Blue-emitting Ir(III) complexes using fluorinated bipyridyl as main ligand and 1,2,4-triazol as ancillary ligand: syntheses, photophysical properties and performances in devices *Tetrahedron* **2016**, *72*, 8335; (c) Wang, C-C.; Jing, Y-M.; Li, T-Y.; Xu, Q-L.; Zhang, S.; Li, W-N.; Zheng, Y-X.; Zuo, J-L.; You, X-Z.; Wang, X-Q. Syntheses, Photoluminescence, and Electroluminescence of Iridium(III) Complexes with Fluorinated 2-Phenylpyridine as Main Ligands and Tertraphenylimidodiphosphinate as Ancillary Ligand *Eur. J. Inorg. Chem.* **2013**, 5683.

(28) Nonoyama, M. Benzo[h]quinolin-10-yl-N Iridium(III) Complexes *Bull. Chem. Soc. Jap.* **1974**, *47*, 767

(29) (a) Tamayo, A.B.; Alleyne, B.D.; Djurovich, P.I.; Lamansky, S.; Tsyba, I.; Ho, N.M.; Bau, R.; Thompson, M.E. Synthesis and characterization of facial and meridional tris-cyclometalated iridium(III) complexes *J. Am. Chem. Soc.* **2003**, *125*, 7377; (b) Lamansky, S.; Djurovich, P.; Murphy, D.; Abdel-Razzaq, F.; Kwong, R.; Tsyba, I.; Bortz, M.; Mui, B.; Bau, R.; Thompson, M.E. Synthesis and characterization of phosphorescent cyclometalated iridium complexes *Inorg. Chem.* **2001**, *40*, 1704; (c) Colombo, M.G.; Brunold, T.C.; Riedener, T.; Gudel, H.U.; Fortsch, M.; Burgi, H-B. Facial tris cyclometalated Rh(III) and Ir(III) complexes – their synthesis, structure, and optical spectroscopic properties *Inorg. Chem.* **1994**, *33*, 545.

(30) Montalti, M.; Credi, A.; Prodi, L.; Gandolfi, M. T. *Handbook of Photochemistry*, Taylor and Francis, Boca Raton, FL, 2006.

(31) Stonelake, T.M.; Phillips, K.A.; Otaif, H.Y.; Edwardson, Z.C.; Horton, P.N.; Coles, S.J.; Beames, J.M.; Pope, S.J.A. Spectroscopic and theoretical investigation of color tuning in deep-red luminescent iridium(III) complexes *Inorg. Chem.* **2020**, *59*, 2266.

(32) Li, X.; Tong, X.; Yongheng, Y.; Yan, H.; Lu, C.; Huang, W.; Zhao, Q. Using highly emissive and environmentally sensitive o-carborane-functionalized metallophosphors to monitor mitochondrial polarity *Chem. Sci.* **2017**, *8*, 5930.

(33) (a) Hasan, K.; Zysman-Colman, E. Panchromic Cationic Iridium(III) Complexes *Inorg. Chem.* **2012**, *51*, 12560; (b) Bokarev, S. I.; Bokareva, O.S.; Kuhn, O. Electronic excitation spectrum of the photosensitizer [Ir(ppy)$_2$(bpy)]$^+$ *J. Chem. Phys.* **2012**, *136*, 214305.

(34) For example: (a) Li, G.M.; Zhu, D.X.; Peng, T.; Liu, Y.; Wang, Y.; Bryce, M.R. Very High Efficiency Orange-Red Light-Emitting Devices with Low Roll-Off at High Luminance Based on an Ideal Host-Guest System Consisting of Two Novel Phosphorescent Iridium Complexes with Bipolar Transport *Adv. Funct. Mater.* **2014**, *24*, 7420; (b) Tsuboyama, A.; Iwawaki, H.; Furugori, M.; Mukaide, T.; Kamatani, J.; Igawa, S.; Moriyama, T.; Miura, S.; Takiguchi, T.; Okada, S.; Hoshino, M.; Ueno, K. Homoleptic cyclometalated iridium complexes with highly efficient red phosphorescence and application to organic light-emitting diode *J. Am. Chem. Soc.* **2003**, *125*, 12971; (c) Su, Y.J.; Huang, H.L.; Li, C.L.; Chien, C.H.; Tao, Y.T.; Chou, P.T.; Datta, S.; Liu, R.S. Highly efficient red electrophosphorescent devices based on iridium isoquinoline complexes: Remarkable external quantum efficiency over a wide range of current *Adv. Mater.* **2003**, *15*, 884; (d) Lai, P-N.; Teets, T.S. Ancillary Ligand Effects on Red-Emitting Cyclometalated Iridium Complexes *Chem. Eur. J.* **2019**, *25*, 6026; (e) Lai, P-N.; Brysacz, Alam, M.K.; Ayoub, N.A.; Gray, T.G.; Bao, J.; Teets, T.S. Highly Efficient Red-Emitting Bis-Cyclometalated Iridium Complexes *J. Am. Chem. Soc.* **2018**, *140*, 10198; (f) Sun, J.; Wu, W.; Zhao, J. Highly Efficient Red-Emitting Bis-Cyclometalated Iridium Complexes *Chem. Eur. J.* **2012**, *18*, 8100; (g) Hasan, K.; Bansal, A.K.; Samuel, I.D.W.; Roldan-Carmona, C.; Bolink, H.J.; Zysman-Colman, E. Tuning the emission of cationic iridium(III) complexes towards the red through methoxy substitution of the cyclometalating ligand *Sci. Rep.* **2015**, *5*, 12325.

(35) Longhi, E.; De Cola, L. Chapter 6. Iridium(III) complexes for OLED application, *in Iridium(III) in Optoelectronic and Photonics Applications* Ed. Zysman-Colman, E. Wiley, 2017.

(36) (a) Ma, D.; Tsuboi, T.; Qiu, Y.; Duan, L. Recent progress in ionic iridium(III) complexes for organic electronic devices *Adv. Mater.* **2017**, *29*, 1603253; (b) Ma, D.; Zhang, C.; Liu, R.; Qiu, Y.; Duan, L. *ACS Appl. Mater. Interfaces* **2018**, *10*, 29814.

(37) Ma, D.; Zhang, C.; Liu, R.; Qiu, Y.; Duan, L. *Chem. Eur. J.* **2018**, *24*, 5574.

(38) Billimoria, J.D.; Maclagan, N.F. Simple analogs of cortisone III. Monocyclic compounds. *J. Chem. Soc.* **1954**, 3257.

(39) Frank, M.; Nieger, M.; Vogtle, F.; Belser, P.; von Zelewsky, A.; de Cola, L.; Balzani, V.; Barigelletti, F.; Flamigni, L. Dinuclear Ru(II) and/or Os(II) complexes of bis-bipyridine bridging ligands containing adamantane spacers: synthesis, luminescence properties, intercomponent energy and electron transfer processes *Inorg. Chim. Acta* **1996**, *242*, 281.

(40) Frisch, M. J.; Trucks, G. W.; Schlegel, H. B.; Scuseria, G. E.; Robb, M. A.; Cheeseman, J. R.; Scalmani, G.; Barone, V.; Mennucci, B.; Petersson, G. A.; Nakatsuji, H.; Caricato, M.; Li, X.; Hratchian, H. P.; Izmaylov, A. F.; Bloino, J.; Zheng, G.; Sonnenberg, J. L.; Hada, M.; Ehara, M.; Toyota, K.; Fukuda, R.; Hasegawa, J.; Ishida, M.; Nakajima, T.; Honda, Y.; Kitao, O.; Nakai, H.; Vreven, T.; Montgomery Jr, J. A.; Peralta, J. E.; Ogliaro, F.; Bearpark, M.; Heyd, J. J.; Brothers, E.; Kudin, K. N.; Staroverov, V. N.; Keith, T.; Kobayashi, R.; Normand, J.; Raghavachari, K.; Rendell, A.; Burant, J. C.; Iyengar, S. S.; Tomasi, J.; Cossi, M.; Rega, N.; Millam, J. M.; Klene, M.; Knox, J. E.; Cross, J. B.; Bakken, V.; Adamo, C.; Jaramillo, J.; Gomperts, R.; Stratmann, R. E.; Yazyev, O.; Austin, A. J.; Cammi, R.; Pomelli, C.; Ochterski, J. W.; Martin, R. L.; Morokuma, K.; Zakrzewski, V. G.; Voth, G. A.; Salvador, P.; Dannenberg, J. J.; Dapprich, S.; Daniels, A. D.; Farkas, O.; Foresman, J. B.; Ortiz, J. V.; Cioslowski, J.; Fox, D. J. *Gaussian 09, Revision C.01*; Gaussian Inc.: Wallingford CT, 2010.

(41) (a) Dunning Jr., T. H.; Hay, P.J. in Modern Theoretical Chemistry, Ed. Schaefer III, H.F. Vol. 3 (Plenum, New York, 1977) 1-28; (b) Kuechle, W.; Dolg, M.; Stoll, H.; Preuss, H. Ab initio pseudopotentials for HG through RN. 1. Parameter sets and atomic calculations *Mol. Phys.* **1991**, *74*, 1245.

(42) Ditchfield, R.; Hehre, W.J.; Pople, J.A. Self-Consistent Molecular Orbital Methods. IX. Extended Gaussian-type basis for molecular-orbital studies of organic molecules *J. Chem. Phys.* **1971**, *54*, 724.

(43) O'Boyle, N.M.; Tenderholt, A.L.; Langner, K.M. cclib: a library for package-independent computational chemistry algorithms. *J. Comput.Chem.* **2008**, *29*, 839

(44) Pettersen, E.F.; Goddard, T.D.; Huang, C.C.; Couch, G.S.; Greenblatt, D.M.; Meng, E.C.; Ferrin, T.E. UCSF Chimera - a visualization system for exploratory research and analysis *J. Comput. Chem.* **2004**, *25*, 1605.

(45) Coles, S.J.; Gale, P.A. Changing and challenging times for service crystallography *Chem. Sci.* **2012**, *3*, 683.

(46) Sheldrick, G.M., ShelXT-Integrated space-group and crystal-structure determination, *Acta Cryst.* **2015**, *A71*, 3.

(47) Dolomanov, O.V.; Bourhis, L.J.; Gildea, R.J.; Howard, J.A.K.; Puschmann, H. Olex2: A complete structure solution, refinement and analysis program, *J. Appl. Cryst.* **2009**, *42*, 339.

(48) Sheldrick, G.M., Crystal structure refinement with ShelXL, *Acta Cryst.* **2015**, *C27*, 3.

(49) Patel, A.M.; Patel, D.J.; Pandya, K.S. Synthesis and antimicrobial activity of some new isopropylquinazolin-4(3H)-one derivatives *Chemica Sinica* **2014**, *5*, 24.

(50) Jeong, K-W.; Lee, J-H.; Park, S-M.; Choi, J-H.; Jeong, D-Y.; Choi, D-H.; Nam, Y.; Park, J-H.; Lee, K-N.; Kim, S-M.; Ku, J-M. Synthesis and in-vitro evaluation of 2-amino-4-arylthiazole as inhibitor of 3D polymerase against foot-and-mouth disease (FMD) *Eur. J. Med. Chem.* **2015**, *102*, 387.

(51) Yi, C.; Chen, J.; Wei, C.; Wu, S.; Wang, S.; Hu, D.; Song, B. alpha-Haloacetophenone and analogues as potential antibacterial agents and nematicides *Bioorg. Med. Chem. Lett.* **2020**, *30*, 126814.

(52) Xia, C.; Wang, D-C.; Qu, G-R.; Guo, H-M. Palladium-catalyzed enantioselective [5+4] annulation of ortho-quinone methides and vinylethylene carbonates *Org. Chem. Front.* **2020**, *7*, 1474.

For Table of Contents ONLY

Acetophenones

2-Phenylquinoxalines

Yellow-to-deep red lumophores
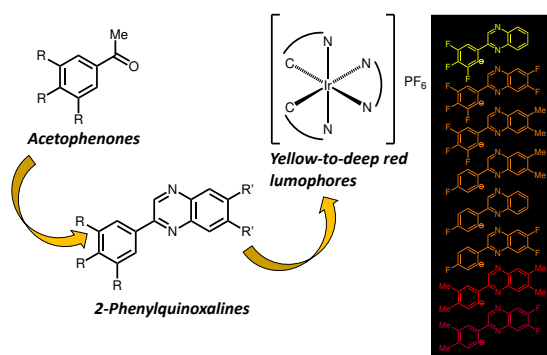
Cationic iridium(III) complexes that incorporate cyclometalated, polysubstituted 2-phenylquinoxaline ligands demonstrate tuneable emission in the yellow-orange-red region of the visible spectrum.